

Supporting Information for

Successful computationally-directed templating of metastable pharmaceutical polymorphs

David H. Case¹, Vijay K. Srirambhatla², Rui Guo¹, Rona E. Watson¹, Louise S. Price¹, Hector Polyzois^{2,3}, Jeremy K. Cockcroft¹, Alastair J. Florence², Derek A. Tocher¹ & Sarah L. Price^{1*}

¹Department of Chemistry, University College London, 20 Gordon Street, London WC1H 0AJ, U.K.

²EPSRC Future Continuous Manufacturing and Advanced Crystallization Hub, University of Strathclyde, Technology and Innovation Centre, 99 George Street, Glasgow, G1 1RD, U.K.

³National Physical Laboratory Scottish Hub, University of Strathclyde, Technology and Innovation Centre, 99 George Street, Glasgow, G1 1RD, U.K.

Table of Contents

S1.	Experimental polymorphs used in analysis.....	3
S1.1	List of Experimental structures	3
S1.2	Disorder in experimental polymorphs	4
S1.3	Packing in experimental structures	4
S1.4	Similarity of experimental structures	6
S2.	The Crystal Structure Prediction (CSP).....	8
S2.1	Conformational profiles	8
S2.2	CrystalPredictor searches	8
S2.3	Refinement of conformations within crystal structures.....	9
S2.4	CrystalOptimizer landscapes.....	11
S2.5	PCM landscapes	12
S3.	Identifying possible isomorphous pairs for targeting.....	12
S3.1	Comparison of the solid solution structures.....	14
S4.	Alternative evaluations of the relative stability of the crystal structures	15
S4.1	Experimental rankings of crystal stability and assessment of accuracy of calculations.....	16
S4.1.1	MFA	16
S4.1.2	TFA	17
S4.1.3	FFA.....	17
S4.1.4	Overall comparisons of energies.....	18

S5.	Nanocrystal surface docking calculations	19
S5.1	Methodology.....	20
S5.2	Docking Results	21
S6.	Solution templating of TFA VI from FFA I.....	22
S7.	Crystallization and powder XRD data.....	23
S7.1	Powder X-ray diffraction	23
S7.1.1	Crystallization of TFA VI	23
S7.1.2	Crystallization of TFA VI from solution by seeding	24
S7.1.3	Co-crystallization of MFA:TFA solid solution	25
S7.1.4	¹ H NMR of MFA:TFA solid solutions.....	26
S7.1.5	Co-crystallization of equimolar amounts of MFA and FFA from solution.....	28
S7.1.6	Crystallization of MFA:FFA solid solution from melt.	28
S7.1.7	Seeding the melt of FFA with MFA:FFA single crystal.....	30
S7.1.8	Co-crystallization of TFA:FFA solid solutions	30
S7.1.9	Crystallization of TFA VII	32
S7.2	Single crystal X-ray diffraction	33
S7.2.1	Complete list of sublimation experiments.....	34
S8.	TFA Form VIII.....	36
S8.1	Preparation of TFA Form VIII.....	36
S8.2	Form VIII crystal structure.....	37
S8.3	Sublimation Studies using QBox	39
S9.	Reproduction of experimental and isostructural crystal cell parameters by various computational models.	42
S10.	CSP Structures.....	48

S1. Experimental polymorphs used in analysis

S1.1 List of Experimental structures

Table S1. Experimental crystal structures of MFA, TFA and FFA, excluding FFA VIII with $Z'=8.5$ which was not included in this study. The torsional angle ϕ is given its value between 0 and 180°, using the approximate mirror symmetry of the acid group. The ordered models derived from the disordered structures are shown in Figure S1.

Polymorph	Z'	Space group	Disorder	CSD refcode & ref.	Temperature	Dihedral Angles $\phi/^\circ$
MFA I	1	P-1		XYANAC ¹	RT	63.6
MFA II	1	P-1	Ring Flip	XYANAC02 ²	150 K	110.5 (104.8)
MFA III	1	P-1		XYANAC03 ³	298 K	100.9
TFA I	1	P21/c		KAXXAI01 ⁴	110 K	107.7
TFA II	1	P21/n		KAXXAI ⁴	110 K	42.2
TFA III	2	P21/c		KAXXAI02 ⁵	85 K	44.2, 57.6
TFA IV	3	P-1		KAXXAI03 ⁵	85 K	67.3, 57.6, 47.8
TFA V	1	P-1	Ring Flip	KAXXAI04 ⁵	85 K	55.6 (77.0)
TFA VI	1	P-1	Ring Slide	S7.2 SCXRD	150 K	62.6 (52.3)
TFA VII	1	P21/n		This work	293 K	117.5
TFA VIII	1	P-1		S8.2 PXRD	120 K	101.2
FFA I	1	P21/c		FPAMCA11 ⁶	RT	53.9
FFA II	1	P21/c		FPAMCA17 ⁷	95 K	42.9
FFA III	1	C2/c		FPAMCA ⁸	RT	176.5
FFA IV	3	P-1	CF ₃ unresolved	FPAMCA15 ⁷	273 K	35.9, 41.8, 156.1
FFA V	4	P21/c		FPAMCA16 ⁷	95 K	40.1, 27.7, 29.0, 37.7
FFA VI	6	P-1		FPAMCA14 ⁷	85 K	33.6, 40.7, 158.2, 158.8, 35.5, 37.5
FFA VII	2	P21/c		FPAMCA12 ⁷	85 K	142.3, 142.6

S1.2 Disorder in experimental polymorphs

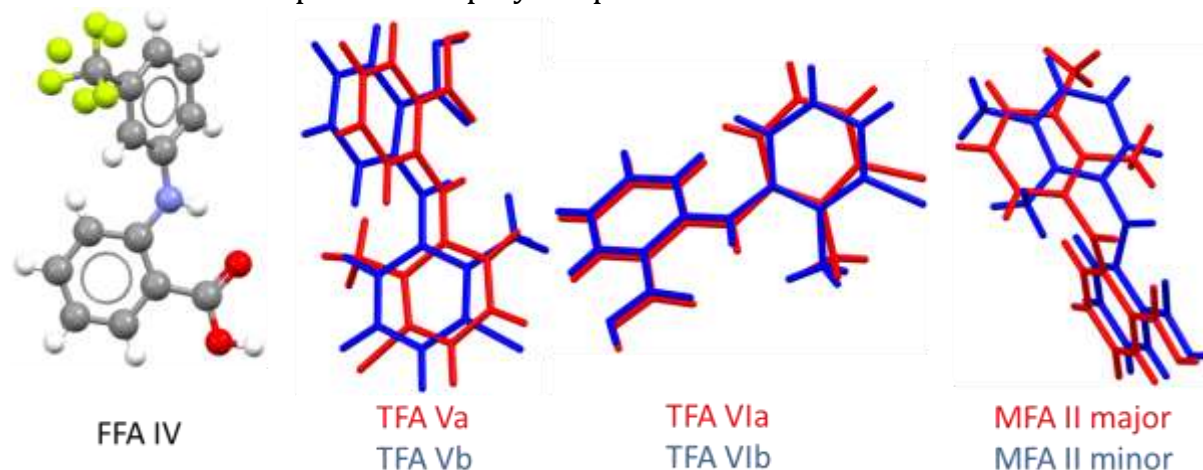


Figure S1. Disordered structures: FFA IV has rotational disorder in CF₃; we used the 1st molecule in .cif with bonds. TFA V and MFA II have a flip in the non hydrogen bonded ring, whereas this ring is rotated in TFA VI. Major and minor components are labelled in MFA II, but the structures are denoted a or b in TFA VI and TFA V. The components of TFA V were not found in the CSP searches, probably because of the distorted geometry around the N atom.

S1.3 Packing in experimental structures

All structures involve the $R_2^2(8)$ COOH dimer, related by inversion, so that the two benzoic acid rings are co-planar. The structures are differentiated by the nearest neighbour packings of the other aromatic ring, which are affected by the chemical changes in the substituents and shown in Figure S2.

In the labelling scheme in Figure S2, positions 1 to 4 denote the non-acidic rings in co-planar geometries. In 1, the substituted groups lie broadside to each other, whilst in 2 the second molecule is rotated 180° around its length to expose the non-substituted positions. In positions 3 and 4, the rings slide in the plane to new positions. In position 5 the CF₃ groups lie approximately along an axis, and in arrangement 6, there is a “T” configuration.

MFA, whose known crystals are all in the P-1 space group, does not pack its dimers in the crystal structure with as wide a range of geometries as TFA and FFA. The most common motif, 1a, is seen in the MFA I structure. The 1' positions, seen in the metastable MFA II major and MFA III, are not seen in TFA or FFA. In these structures the two Me groups are kept in contact, but displaced to be either above or below each other. In the MFA structures, the non-acidic rings are always co-planar with neighbours.

TFA has a wider range of dimer substituent interactions, and has proven to be more adaptable in the templating experiments presented here. TFA form VII is unusual in that the non-acidic rings are not co-planar, but have the Cl pointing to the aromatic ring. This is the main packing difference between the MFA solid solution structures (MFA I) and the TFA:FFA solid solution (ESI Figure S7).

FFA has the ability to take on many structures, it has more structurally characterized polymorphs than any other system at the time of writing,⁷ and contains geometries which are quite unlike those of MFA and TFA. One of these, 5b, is the most thermodynamically stable at low temperature, and will compete with templating targets from TFA or MFA. Some of its structures contain asymmetric

molecules in markedly different environments, and there are many $Z' > 1$ structures that contain molecules with very different dihedral angles.

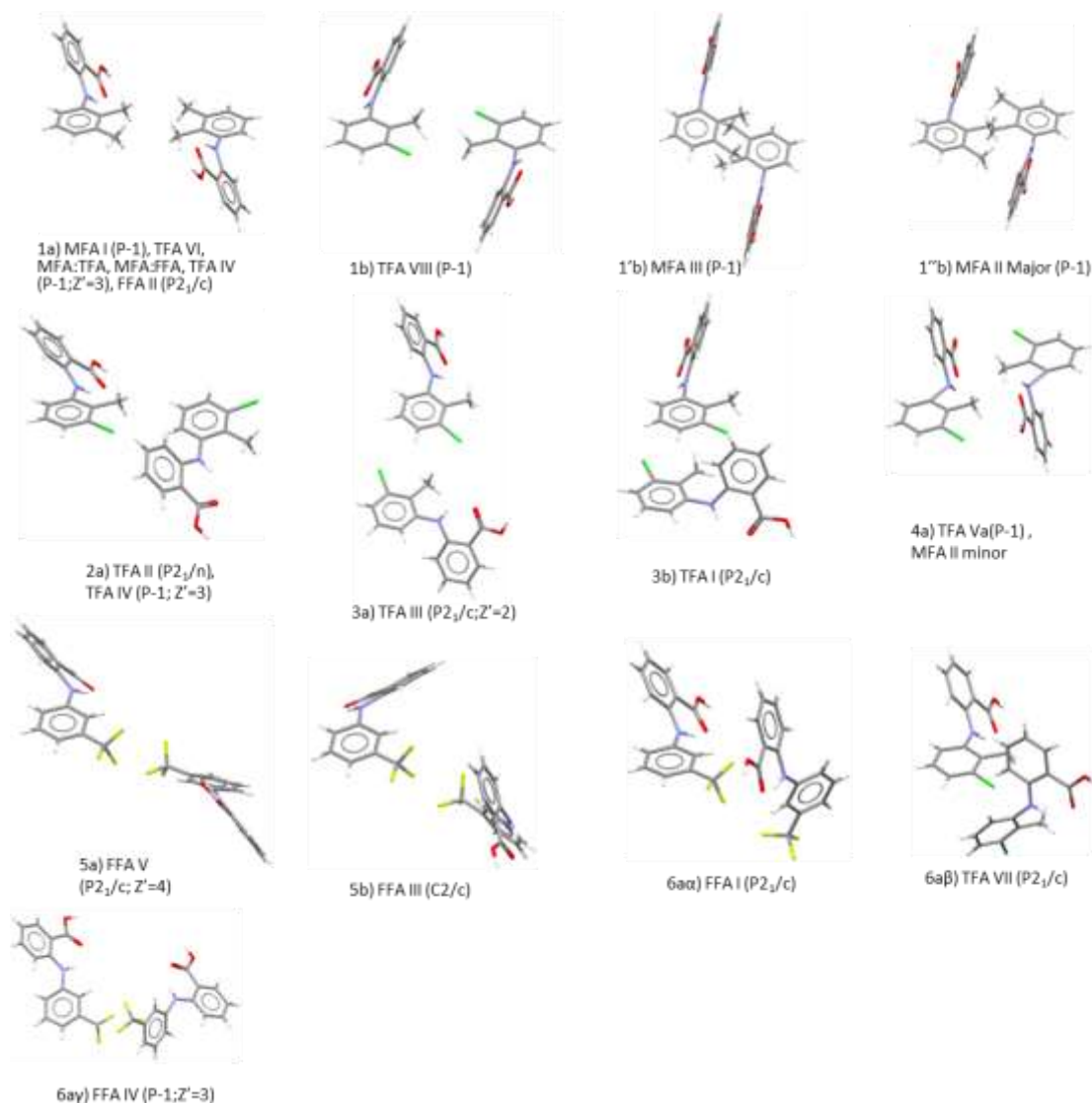


Figure S2. Classification of substituent interactions as exemplified by the dimers in the experimental structures. Each interaction motif structures in which it is found, with the space group and Z' value if greater than 1 by the first structure and any others where this differs. The alphanumeric label is a composite of a number, which denotes the relative position of the substituted aromatic rings and a letter which denotes whether the molecule is in the lower (a) or higher (b) angle dihedral well (Figure S3). Cases 1b have different displacements indicated by primes, and 6a has a Greek letter to differentiate twists of the second molecule. Not all of the asymmetric environments which appear in some of the $Z' > 1$ structures are shown.

S1.4 Similarity of experimental structures

The similarity of the fenamate polymorphs, as quantified by the optimal RMSD(n) calculated using the Crystal Similarity tool in Mercury. This data is graphically summarised in Figure 8 of the manuscript. Table S2 - Table S4 compare the polymorphs of each molecule, and Table S5 - Table S7 compare the polymorphs of different molecules.

Table S2. Optimal, by RMSD, overlays of up to 15 molecules for MFA vs MFA polymorphs. Cells display the number of matches, *n*, and the RMSD(*n*) / Å in parentheses.

	MFA I	MFA II	MFA III
MFA I	15 (0.00)	3 (1.04)	3 (0.76)
MFA II	3 (1.04)	15 (0.00)	2 (0.08)
MFA III	3 (0.76)	2 (0.08)	15 (0.00)

Table S3. Optimal, by RMSD, overlays of up to 15 molecules for TFA vs TFA polymorphs. Cells display the number of matches, *n*, and the RMSD(*n*) / Å in parentheses.

	TFA I	TFA II	TFA III	TFA IV	TFA V	TFA VI	TFA VII	TFA VIII
TFA I	15 (0.00)	1 (0.87)	2 (0.77)	2 (0.69)	2 (0.45)	2 (0.65)	2 (0.68)	11 (0.15)
TFA II	1 (0.87)	15 (0.00)	2 (0.28)	2 (0.32)	1 (0.58)	2 (0.33)	2 (0.30)	1 (0.85)
TFA III	2 (0.77)	2 (0.28)	15 (0.00)	11 (0.48)	2 (0.58)	11 (0.48)	11 (0.30)	2 (0.73)
TFA IV	2 (0.69)	2 (0.32)	11 (0.48)	15 (0.00)	3 (0.62)	14 (0.37)	11 (0.36)	3 (0.63)
TFA V	2 (0.45)	1 (0.58)	2 (0.58)	3 (0.62)	15 (0.00)	4 (0.73)	3 (0.62)	4 (0.91)
TFA VI	2 (0.65)	2 (0.33)	11 (0.48)	14 (0.37)	4 (0.73)	15 (0.00)	11 (0.25)	3 (0.68)
TFA VII	2 (0.68)	2 (0.30)	11 (0.30)	11 (0.36)	3 (0.62)	11 (0.25)	15 (0.00)	2 (0.64)
TFA VIII	11 (0.15)	1 (0.85)	2 (0.73)	3 (0.63)	4 (0.91)	3 (0.68)	2 (0.64)	15 (0.00)

Table S4. Optimal, by RMSD, overlays of up to 15 molecules for FFA vs FFA polymorphs. Cells display the number of matches, *n*, and the RMSD(*n*) / Å in parentheses.

	FFA I	FFA II	FFA III	FFA IV	FFA V	FFA VI	FFA VII
FFA I	15 (0.00)	2 (0.51)	1 (1.34)	3 (0.97)	4 (0.55)	3 (0.95)	1 (1.08)
FFA II	2 (0.51)	15 (0.00)	1 (1.31)	2 (0.17)	2 (0.61)	2 (0.20)	1 (1.14)
FFA III	1 (1.34)	1 (1.31)	15 (0.00)	2 (0.54)	1 (1.45)	2 (0.55)	2 (0.52)
FFA IV	3 (0.97)	2 (0.17)	2 (0.54)	15 (0.00)	2 (0.64)	13 (0.22)	1 (0.27)
FFA V	4 (0.55)	2 (0.61)	1 (1.45)	2 (0.64)	15 (0.00)	3 (0.81)	1 (1.20)
FFA VI	3 (0.95)	2 (0.20)	2 (0.55)	13 (0.22)	3 (0.81)	15 (0.00)	1 (0.25)
FFA VII	1 (1.08)	1 (1.14)	2 (0.52)	1 (0.27)	1 (1.20)	1 (0.25)	15 (0.00)

Table S5. Optimal, by RMSD, overlays of up to 15 molecules for TFA vs MFA polymorphs. Cells display the number of matches, n , and the RMSD(n) / Å in parentheses.

	MFA I	MFA II	MFA III
TFA I	2 (0.56)	2 (0.09)	5 (0.18)
TFA II	2 (0.29)	1 (0.71)	1 (0.68)
TFA III	11 (0.39)	1 (0.59)	2 (0.59)
TFA IV	14 (0.32)	3 (0.94)	2 (0.54)
TFA V	4 (0.68)	7 (0.97)	3 (0.40)
TFA VI	15 (0.13)	2 (0.68)	2 (0.50)
TFA VII	11 (0.18)	2 (0.70)	2 (0.52)
TFA VIII	3 (0.59)	3 (0.38)	5 (0.23)

Table S6. Optimal, by RMSD, overlays of up to 15 molecules for MFA vs FFA polymorphs. Cells display the number of matches, n , and the RMSD(n) / Å in parentheses.

	FFA I	FFA II	FFA III	FFA IV	FFA V	FFA VI	FFA VII
MFA I	5 (0.18)	2 (0.20)	1 (0.77)	2 (0.22)	4 (0.54)	3 (0.98)	1 (0.58)
MFA II	2 (0.45)	1 (0.47)	2 (0.62)	2 (0.51)	1 (0.51)	2 (0.53)	3 (0.37)
MFA III	2 (0.42)	2 (0.49)	2 (0.64)	2 (0.48)	2 (0.64)	2 (0.50)	2 (0.40)

Table S7. Optimal, by RMSD, overlays of up to 15 molecules for TFA vs FFA polymorphs. Cells display the number of matches, n , and the RMSD(n) / Å in parentheses.

	FFA I	FFA II	FFA III	FFA IV	FFA V	FFA VI	FFA VII
TFA I	2 (0.48)	2 (0.55)	2 (0.59)	2 (0.54)	2 (0.69)	3 (0.63)	2 (0.34)
TFA II	2 (0.15)	2 (0.10)	1 (0.89)	2 (0.16)	2 (0.40)	3 (1.71)	2 (1.03)
TFA III	5 (0.25)	2 (0.22)	1 (0.81)	2 (0.24)	4 (0.52)	3 (0.90)	1 (0.64)
TFA IV	5 (0.34)	2 (0.20)	1 (0.76)	2 (0.23)	3 (0.46)	3 (0.84)	1 (0.57)
TFA V	2 (0.37)	2 (0.42)	2 (0.87)	2 (0.38)	2 (0.55)	2 (0.40)	3 (0.61)
TFA VI	5 (0.16)	2 (0.20)	1 (0.77)	2 (0.19)	4 (0.53)	2 (0.21)	1 (0.58)
TFA VII	5 (0.19)	2 (0.17)	1 (0.81)	2 (0.19)	4 (0.49)	2 (0.21)	1 (0.61)
TFA VIII	2 (0.46)	1 (0.48)	2 (0.62)	2 (0.65)	1 (0.53)	3 (0.68)	3 (0.68)

S2. The Crystal Structure Prediction (CSP)

S2.1 Conformational profiles

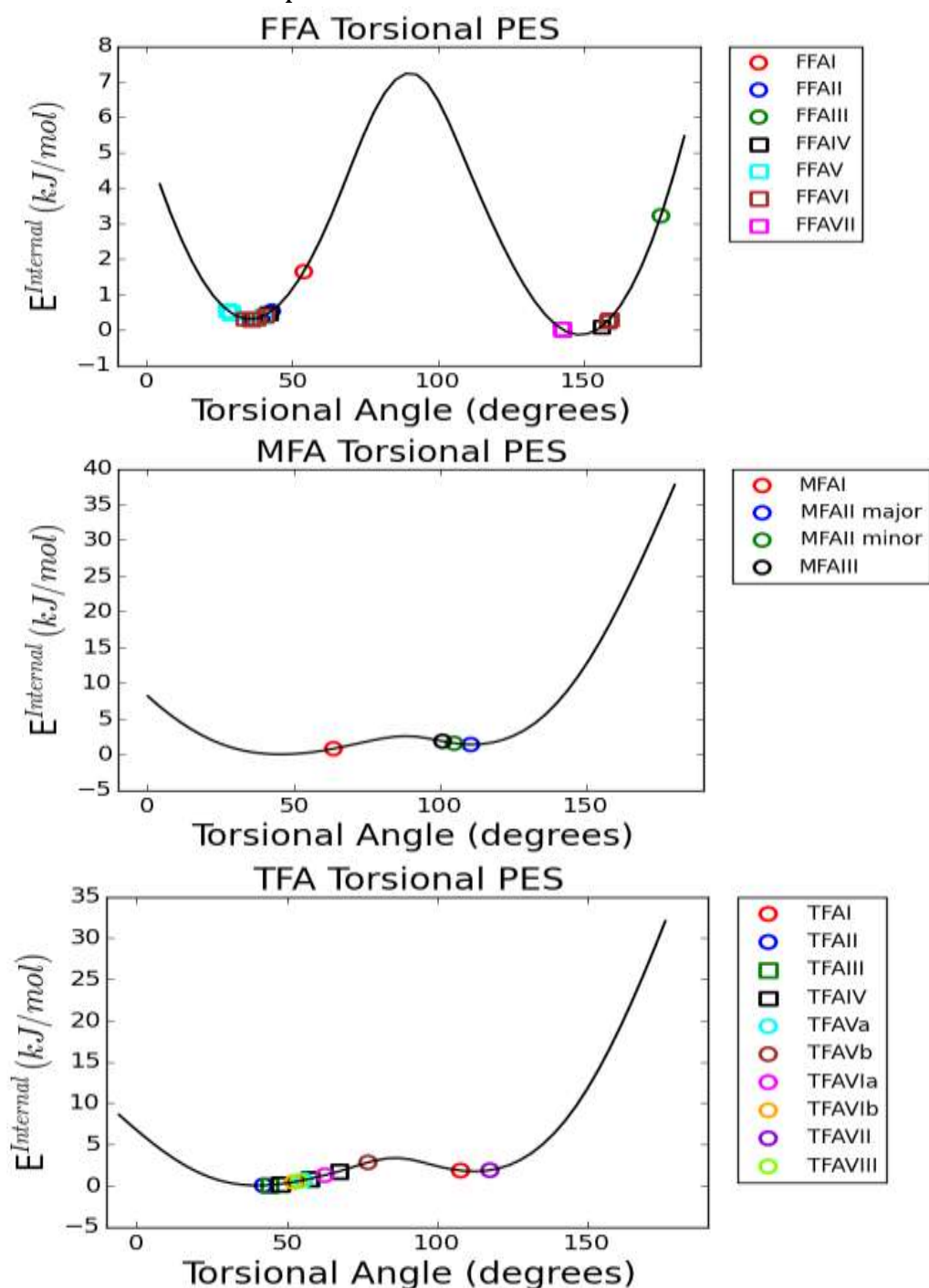


Figure S3. The conformational potential energy of each molecule at the PBE0/6-31+G(d) level of theory using Gaussian09⁹ with the primary dihedral angle ϕ only constrained between 0 and 180°. The PES, in black, is a cubic spline interpolation between points separated by 15 degrees. The experimental polymorphs, which are represented by circles in the case of $Z'=1$ structures, and squares otherwise.

S2.2 CrystalPredictor searches

Structures were generated for $Z'=1$ in the space groups P1, P-1, P2₁, P2₁/C, P2₁2₁2, P2₁2₁2₁, PNA2₁, PCA2₁, PBCA, PBCN, C2/C, CC, C2, PC, CM, P2₁/M, C2/M, P2/C, C222₁, PMN2₁, CMC2₁, ABA2, FDD2, IBA2, PNNA, PCCN, PBCM, PNNM, PMMN, PNMA, CMCM, CMCA, FDDD, IBAM, P4₁, P4₃, I-4,

P4/N, P42/N, I4/M, I41/A, P4₁2₁2, P4₃2₁2, P-42₁C, I-42D, P3₁, P3₂, R3, P-3, R-3, P3₁21, P3₂21, R3C, R-3C, P6₁, P6₃, P6₃/M, P2₁3 and PA-3. The maximum allowed unit cell length in the FFA search was 32 Å, which meant that FFA III with $a=39.85 \text{ \AA}$ was not found in the search.

The search variables included ϕ using the torsional profiles in to estimate the intramolecular energy penalty ΔE_{intra} . The intermolecular contribution to the lattice energy U_{inter} was calculated by the FIT exp-6 repulsion-dispersion potential with the CHELPG atomic charges at the lowest energy molecular conformation. The lattice energy is given by the expression $E_{\text{latt}}=\Delta E_{\text{intra}}+U_{\text{inter}}$

S2.3 Refinement of conformations within crystal structures

The lowest energy structures underwent further optimization of the conformation variables in response to the packing forces. CrystalOptimizer was used to perform the lattice energy optimization by coupling GAUSSIAN09 molecular wavefunction evaluations and DMACRYS lattice optimizations, with distributed multipoles used to express the electrostatic contribution to U_{inter} . The use of databases of the ab-initio data made this computationally feasible. The conformational variables considered are defined by the atomic numbering in Figure S4.

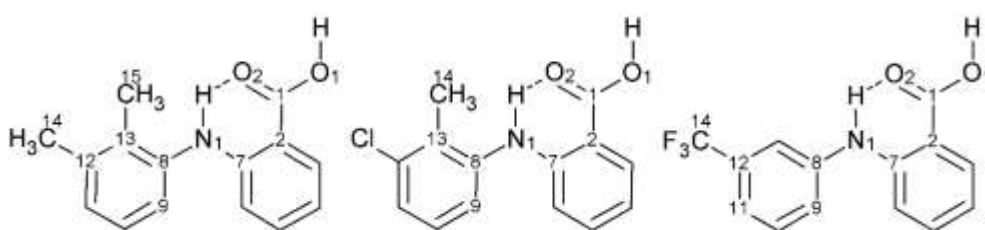


Figure S4. Atomic numbering system for fenamic acids. MFA, TFA and FFA. ϕ (C7-N1-C8-C9) is zero for the planar conformation shown.

CrystalOptimizer explicitly optimized the selected dihedrals and a few bond angles, given below, with the other degrees of freedom being determined by the isolated molecule constrained optimization. The lists of atom strings are prefixed by + when the optimization algorithm uses gradients in this direction.

- FFA: +O₁C₁C₂C₇, +H₁O₁C₁C₂, +C₁C₂C₇N₁, +C₇N₁C₈C₉, +H₆N₁C₈C₉, +F₁C₁₄C₁₂C₁₁, +H₆N₁C₈, +H₁O₁C₁
- MFA: +H₁O₁C₁C₂, +O₁C₁C₂C₇, +C₂C₇N₁C₈, +C₇N₁C₈C₁₃, H₁₄C₁₅C₁₃C₈, H₁₁C₁₄C₁₂C₁₃, +H₆N₁C₈C₁₃, +H₁O₁C₁, +H₁N₁C₈
- TFA: +H₁O₁C₁C₂, +O₁C₁C₂C₇, +C₂C₇N₁C₈, +C₇N₁C₈C₁₃, H₁₁C₁₄C₁₃C₈, +H₆N₁C₈C₁₃, H₁O₁C₁, H₆N₁C₈

For MFA and TFA an intermediate step to use the multipolar electrostatics was used to reduce the number of structures that required being optimized by CrystalOptimizer. Structures where the eigenvalues of the Hessian has imaginary frequencies had their symmetry lowered until they were minima. At various stages, duplicate structures were removed by clustering: CrystalPredictor has an internal algorithm¹⁰ for the initial removal of duplicates, and further identical structures were removed after the CrystalOptimizer stage by an in-house code which is based on finding overlapping clusters of 15 molecules using the same algorithm that has been used for this purpose throughout this work (see section: Identifying possible isomorphous pairs for targeting below).

The crystal energy landscapes at this stage are shown in Figure S5. A final energy evaluation approximated the polarization of the molecules within the crystal structure by recalculating the electrostatic multipole distribution and the intramolecular energy is considered by using the polarizable continuum model (PCM) within Gaussian⁹ with a dielectric constant of $3.0\epsilon_0$, and is

shown in Figure S6. The baseline with respect to which all intramolecular energies are given at the PCM level is the lowest intramolecular energy found in the whole set of CSP structures.

Table S8. Summary of the CSP searches.

	Mefenamic acid	Tolfenamic acid	Flufenamic acid
Gas phase geometry optimization	PBE-0/6-31+G(d)	B3LYP/6-31G(d,p)	B3LYP/6-31G(d,p)
Number of CrystalPredictor structures	1000000	1000000	1000000
Intramolecular model (CrystalPredictor)	B3LYP/6-31G(d,p)	B3LYP/6-31G(d,p)	B3LYP/6-31G(d,p)
Intermolecular model (CrystalPredictor)	ChelpG B3LYP/6-31G(d,p) FIT	ChelpG B3LYP/6-31G(d,p) FIT	ChelpG B3LYP/6-31G(d,p) FIT
Reranking method	DMAflex-quick	DMAflex-quick	None
Intramolecular model (Reranking)	B3LYP/6-31G(d,p)	B3LYP/6-31G(d,p)	N/A
Intermolecular model (Reranking)	GDMA PBE0/6-31+G(d) FIT	GDMA PBE0/6-31G(d,p) FIT	N/A
Intramolecular model (CrystalOptimizer)	PBE0/6-31+G(d)	PBE0/6-31+G(d)	PBE0/6-31+G(d)
Intermolecular model (CrystalOptimizer)	GDMA PBE0/6-31+G(d) FIT	GDMA PBE0/6-31+G(d) FIT	GDMA PBE0/6-31+G(d) FIT
PCM Intramolecular model	PBE0/6-31+G(d) PCM $\epsilon_0=3.0$	PBE0/6-31+G(d) PCM $\epsilon_0=3.0$	PBE0/6-31+G(d) PCM $\epsilon_0=3.0$
PCM Intermolecular model	GDMA PBE0/6-31+G(d) PCM $\epsilon_0=3.0$ FIT	GDMA PBE0/6-31+G(d) PCM $\epsilon_0=3.0$ FIT	GDMA PBE0/6-31+G(d) PCM $\epsilon_0=3.0$ FIT

S2.4 CrystalOptimizer landscapes

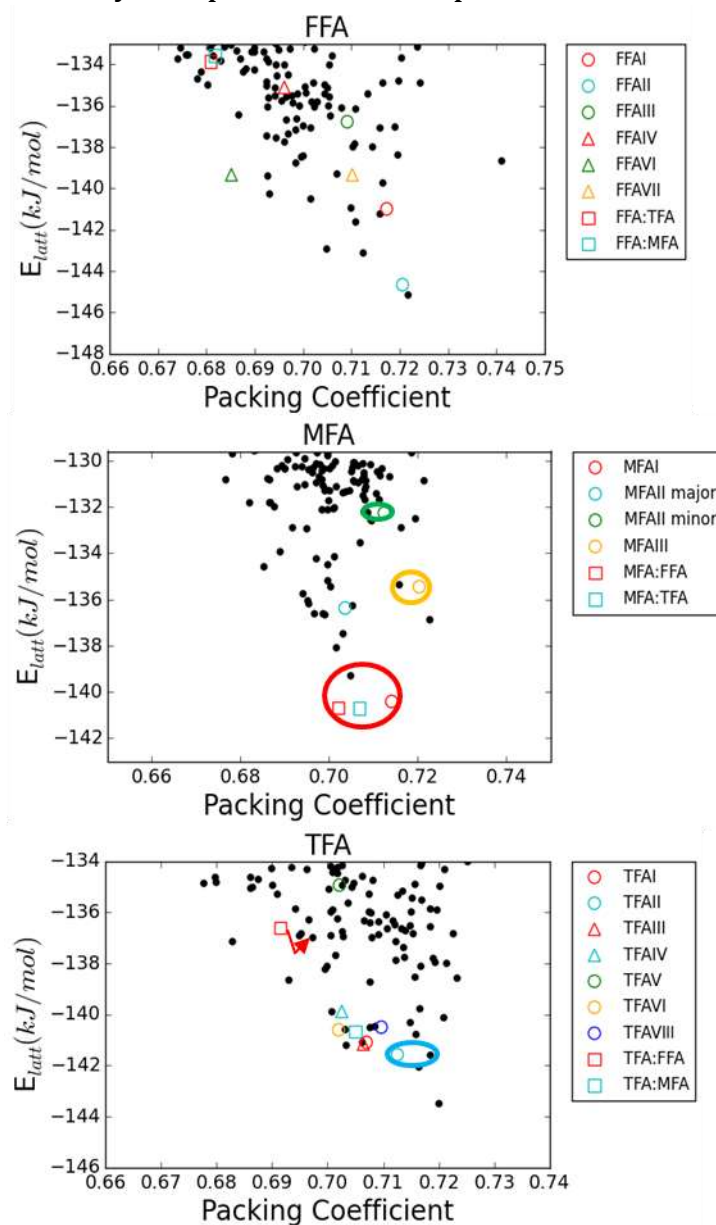


Figure S5. Crystal energy landscapes for the three molecules at the CrystalOptimizer stage. Experimental structures are shown by hollow shapes: circles for $Z'=1$, triangles for $Z'>1$ and squares for solid solutions. In cases for which computationally generated structures (black) match an experimental point, but do not clearly overlay each other on the graph, an exaggerated shape couples the two, or in the case of the TFA:FFA solid solution in TFA, an arrow is used to avoid ambiguity. TFA VII is isomorphous with TFA:FFA.

S2.5 PCM landscapes

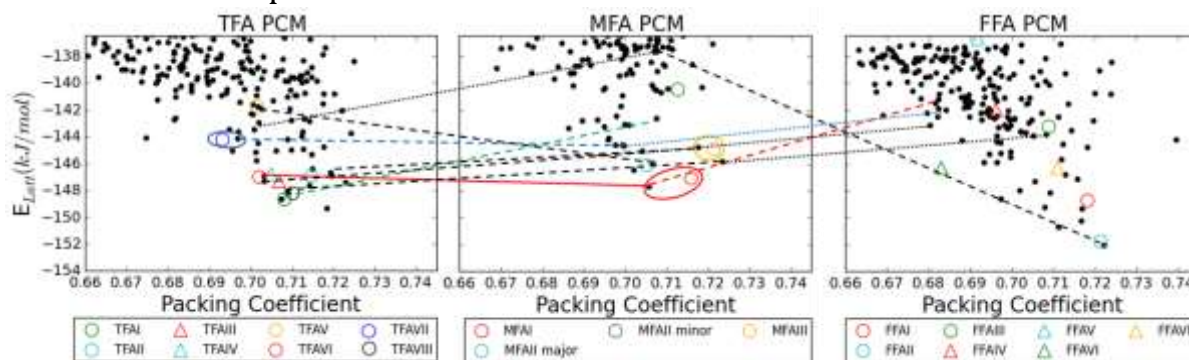


Figure S6. The crystal energy landscapes for the molecules calculated at the PCM level of theory. The tie-lines are the same as those in Figure S2 of the main text, i.e. solid lines indicate both end-points can be realized as polymorphs, dashed lines indicate one end-point is known and dotted lines link hypothetical polymorphs. The red line is isostructural with MFA I, the blue line with TFA VII and the green line TFA I.

S3. Identifying possible isomorphous pairs for targeting

Similarity of experimental forms to CSP structures on the crystal energy landscape Crystal structures were compared by determining the number n of molecules matched ($n \leq 15$) and the RMSD_n overlay (in Å) using the CSD Python API version 1.3.0 Crystal Similarity Tool,¹¹ using default settings, including allowing for molecular differences when appropriate.

The diagonal blocks (comparing polymorphs and CSP structures with the same molecules) in ESI Table S9 show how closely the polymorphs were found in the $Z'=1$ search. The majority of the $Z'=1$ structures were found, though with some differences in the structure which could be attributed to convergence problems on the shallow potential energy surface. TFA IV and VI have the same closest match within $Z'=1$ CSP structures, as may have been anticipated from their similarity. The only $Z'=1$ structures which were not found (* in Table S9) were FFA III whose long unit cell was beyond the bounds set for the initial structure generation algorithm, and the two disorder components of TFA V which both had distorted bonding around the N atom where the closest matching structure T7232 could not match all 15 molecules in the disordered components.

The off-diagonal blocks in Table S9 show whether there is an unknown structure that has a close structural match with a known form. The known forms of FFA do not match any low energy structures of MFA or TFA, with the exception of FFA II having some rather metastable hypothetical analogues on the MFA and TFA landscapes. The structural matches where a stable template is available have been investigated in the manuscript. In addition, TFA III, VII and VIII have CSP generated MFA and FFA structures common across the group, but would be predicted to be far more useful as seeds for MFA than FFA on energetic grounds. MFA and TFA do have matches between all their structures except for some disorder components, but many of these are too high in energy to be likely to be formed even if the experiment could be done.

The solid solutions are also included in this analysis; when overlaying clusters of molecules, the better match with either of the solid solution structure end-points is given (in theory the algorithm should discount molecular differences, but numerically there are differences). Although MFA:TFA and MFA:FFA have the same P-1 structure, which is isomorphous with MFA form I, many of these matches are quite poor and where $\text{RMSD}_n > 0.5$ Å the results of the algorithm are rather ambiguous. The pure FFA end-points of the solid solutions look energetically unfeasible. The two solid solution structures, with the new TFA VII are compared in Section S7.

Table S9. The best match of any structure in each molecule's CSP search (within 15 kJ/mol of the global minimum) to any known polymorph or solid solution. The number of matching molecules n in a cluster of 15, and the $RMSD_n$ in Å is given for the CSP ID (lists of which are given in Section S10). ΔE_{latt} is the energy difference with respect to the global minimum with the PCM energy model. Structures where a 15 molecule overlay was found between all three molecules are in yellow, pairs in blue. Within these bands, structures highlighted in orange (Column 1) indicate the polymorph is suitable for use as a template, structures marked in green indicate where templating experiments inspired by this work produced novel polymorphs, and structures highlighted in red indicate where templating experiments inspired by this work failed to produce the targeted forms. *Cases where structures were not found in the search, where the optimized experimental structure was used for n (RMSD) and ΔE_{latt} .

Polymorph	Space group	Z'	MFA			TFA			FFA		
			n (RMSD)	CSP ID	ΔE_{latt} kJ/mol	n (RMSD)	CSP ID	ΔE_{latt} kJ/mol	n (RMSD)	CSP ID	ΔE_{latt} kJ/mol
MFA I	P-1	1	15 (0.23)	M128	0.00	15 (0.46)	T917=VI	2.39	14 (0.72)	F1129	10.83
MFA II maj	P-1	1	15 (0.35)	M889	1.75	15 (0.15)	T7232	7.56	6 (1.19)	F1242	13.97
MFA II min	P-1	1	15 (0.50)	M497	7.02	7 (0.85)	T646	5.85	6 (0.99)	F1484	9.85
MFA III	P-1	1	15 (0.47)	M1666	2.93	15 (0.78)	T3074	2.62	5 (0.56)	F991	10.96
TFA I	P2 ₁ /c	1	15 (0.40)	M5643	5.06	15 (0.31)	T4121	0.64	11 (1.07)	F882	8.95
TFA II	P2 ₁ /n	1	15 (0.32)	M2104	13.45	15 (0.26)	T283	2.40	8 (1.14)	F32	8.48
TFA III	P2 ₁ /c	2	15 (0.36)	M288	2.65	15 (0.28)	T93	2.00	15 (0.47)	F1248	8.91
TFA IV	P-1	3	14 (0.37)	M128=I	0.00	14 (0.61)	T917 ~ VI	2.39	13 (0.71)	F1129	10.83
TFA V a	P-1	1	15 (0.55)	M497	7.02	15 (0.3)	*	8.58	4 (0.55)	F1173	10.03
TFA V b	P-1	1	11 (0.39)	M889	1.75	15 (1.5)	*	6.60	5 (0.56)	F45	9.80
TFA VI a	P-1	1	15 (0.20)	M128=I	0.00	15 (0.48)	T917	2.39	14 (0.71)	F1129	10.83
TFA VI b	P-1	1	15 (0.31)	M128=I	0.00	15 (0.49)	T917	2.39	14 (0.77)	F1129	10.83
TFA VII	P2 ₁ /n	1	15 (0.34)	M2853	3.05	15 (0.68)	T4809	5.21	15 (0.32)	F1173	10.03
TFA VIII	P-1	1	15 (0.47)	M510	1.85	15 (0.03)	T2	1.16	15 (0.66)	F1956	8.22
FFA I	P2 ₁ /c	1	15 (0.89)	M1971	12.62	11 (0.51)	T1646	11.69	15 (0.17)	F560	2.67
FFA II	P2 ₁ /c	1	15 (0.29)	M1634	10.04	15 (0.25)	T158	5.84	15 (0.11)	F748	0.00
FFA III	C2/c	1	2 (0.47)	M5471	8.23	3 (0.60)	T535	11.09	15 (0.16)	*	8.83
FFA IV	P-1	3	5 (0.78)	M1823	14.23	7 (1.14)	T1152	14.00	6 (0.40)	F1499	6.16
FFA V	P2 ₁ /c	4	7 (1.02)	M2968	9.03	5 (0.92)	T1283	3.53	5 (0.60)	F908	13.74
FFA VI	P-1	6	7 (1.17)	M900	14.71	6 (1.20)	T1646	11.69	6 (0.43)	F1228	9.57
FFA VII	P2 ₁ /c	2	7 (1.06)	M314	12.07	8 (1.35)	T559	5.34	5 (0.58)	F991	10.96
MFA:TFA	P-1	1	15 (0.24)	M128=I	0.00	15 (0.47)	T917	2.39	15 (0.70)	F1129	10.83
MFA:FFA	P-1	1	15 (0.56)	M128=I	0.00	15 (0.56)	T917	2.39	15 (0.22)	F1129	10.83
FFA:TFA	P2 ₁ /c	1	15 (0.40)	M2853	3.05	15 (0.78)	T4809=VIII	5.21	15 (0.21)	F1173	10.03

S3.1 Comparison of the solid solution structures

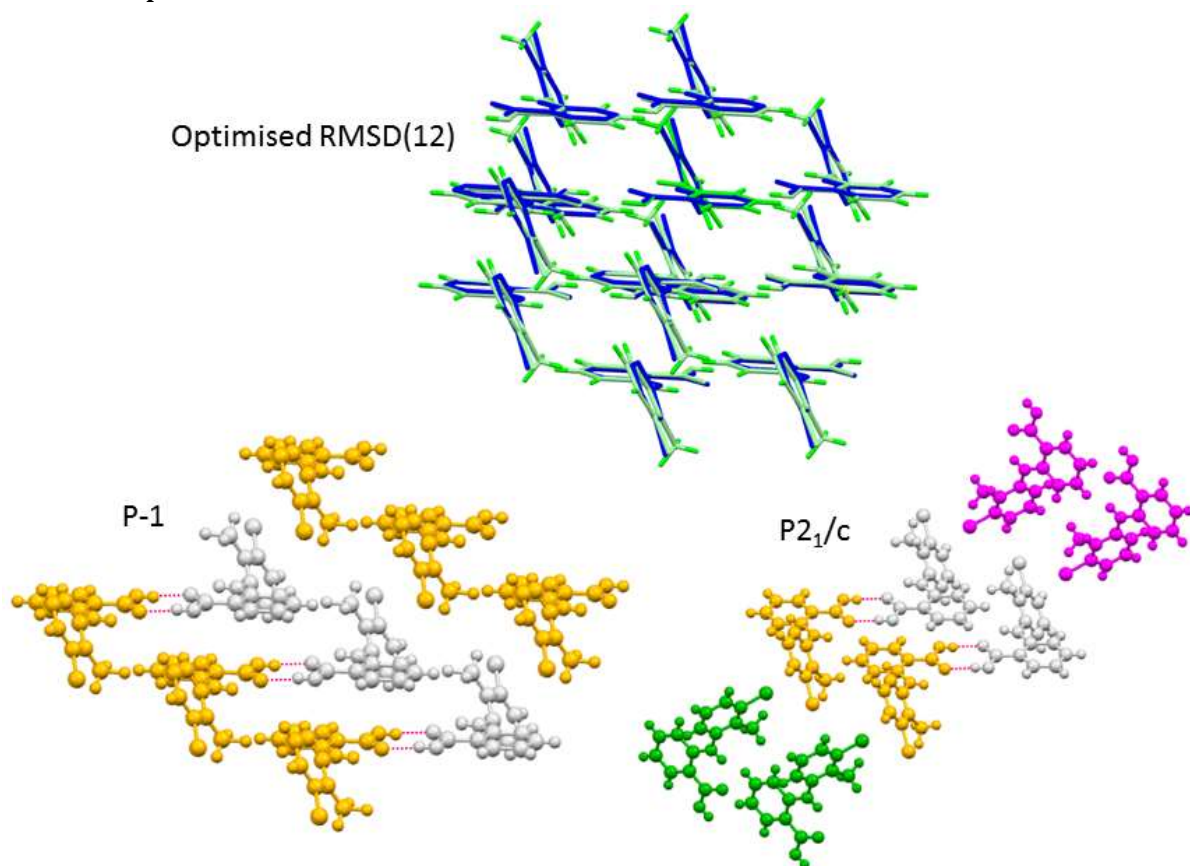


Figure S7. The two solid solution structures illustrated as TFA VI and VII. TFA VI (P-1) is isomorphous with the MFA:TFA and MFA:FFA solid solutions and MFA I. TFA VII is the P2₁/c structure which is isomorphous with the TFA:FFA solid solution. The top graphic displays the optimal overlay by RMSD of 12 molecules (RMSD (12)=0.19 Å) between the two structures. On the left is the P-1 structure in which the molecules related by translation (silver) share close contacts with inverted molecules (gold). Intermolecular hydrogen bonds, shown in red, link pairs of molecules whose acidic rings are co-planar, whilst the non-acidic rings lie co-planar with another molecule; this arrangement is labelled 1a in Figure S2. The same relationship is seen between the hydrogen bonded rings in the P2₁/c structure on the right, however the molecules from the glide (purple) and screw (green) operators change the non-acidic ring geometry to be of type 6aβ by our labelling system. An alternate view of these structures is shown in Figure S9.

S4. Alternative evaluations of the relative stability of the crystal structures

In order to check the sensitivity of the relative energies to the computational assumptions, markedly more expensive periodic electronic structure calculations were performed on the experimental polymorphs and the corresponding structures containing the other molecules found by comparing the crystal energy landscapes. The structures were optimized at the PBE-TS level¹² using CASTEP¹³ with on-the-fly ultrasoft pseudo-potentials and plane wave cutoffs of 900 eV for MFA and TFA, and 1100 eV for FFA. To test the sensitivity to the dispersion correction, the energy of these structures was also evaluated with the MBD* dispersion correction.¹⁴ These energies and structures are compared with the structures generated in the CSP search at the CrystalOptimizer stage (CO, Figure S5), and with rigid-molecule minimization with the intramolecular energies and distributed multipoles recalculated in a polarizable continuum (PCM Figure S6). For these rigid-molecule structures, it was possible to estimate the differences in free energy under a harmonic approximation to the rigid-molecule lattice modes (CO+FE).¹⁵

The relative energies of the structures are compared in Table S10, and the reproduction of the experimental cell parameters by the various methods are shown in Table S22, Table S23, and Table S24. The greatest deviations between the cell lengths of an experimental structure and an equivalent structure after it has been optimized by a model are associated with structures in which the disorder cannot be resolved experimentally. Over the set of 10 structures which have $Z'=1$, with no disorder, and which contain the “native” molecule in the asymmetric unit (those which appear in Figure 6 of the manuscript) the mean (and standard deviation) differences between model and experimental cell lengths have been calculated: these are 0.05 Å (0.34 Å) after CrystalOptimizer optimization, 0.03 Å (0.32 Å) for PCM and -0.04 Å (0.29 Å) for PBE-TS. Whilst the periodic PBE-TS optimizations have the slightly lower standard deviation, the neglect of zero-point energy and thermal expansion in the calculations results in slightly shorter unit cell lengths for this model, whereas the experiments were carried out at 85 K or higher (Table S1) and the force-field calculations, which are parameterized to reproduce structures at experimental temperatures,¹⁶ benefit from a cancellation of errors in this regard. However, given the neglect of thermal expansion, all the structures are reasonably close to their experimental values, for all methods, confirming that the CSP methods are adequately reproducing the structures.

Optimizing MFA I starting from the experimental structure gave a structure that had a lower lattice energy (by 1 kJ/mol at CO stage) than the structure found in the search that also was a good match to MFA I, and there are also differences from the structure using the solid solution starting points. This shows that the potential well corresponding to MFA I is broad, with multiple local minima and probably barriers that are small enough to be averaged over by the vibrations of the molecule. This will mean that the rigid-molecule free energy estimate is very poor, as it does not sample the extent of the energy well, nor allow the low frequency librations of the phenyl rings to couple with the lattice modes, though it does increase the energy difference by 0.5 kJ/mol between various representations of the MFA I structure. Hence, the neglect of thermal and zero-point effects is a significant limitation in comparing static lattice energies for these molecules with experimental stability data.

Table S10. Relative energies of the isostructural analogues of each experimental polymorph, in kJ/mol, relative to a baseline. The energies are relative to the lowest energy structure found in the CSP for the atomistic models giving the energies after CrystalOptimizer (CO), with ΔE_{intra} and multipoles from a polarizable continuum model (PCM), and with a rigid-molecule free energy estimate at 298 K (CO+FE). The energy of the molecular conformation (PBE0/6-31+G(d)) relative to the optimized conformation, ΔE_{intra} , is also given. Energies from periodic DFT calculations are given, for a geometry optimized at the PBE-TS level, with a further single point energy at PBE-MBD*. The lattice energies are given relative to the most stable low temperature polymorph, i.e. MFA I, TFA II, and FFA III. The columns headed 'Source of Structure' denote whether the starting structure is an experimental structure E (Table S1), or CSP generated structure ID (Table S9), or when an isostructural match was not found in the CSP, P denoting the pasting of the molecular structure into the crystal. Certain calculations are italicized: this denotes that only one calculation was performed for two or more isomorphous experimental structures. Blank entries occur where the energy has not been calculated, because the experimental structures have disorder which has not been resolved into separate components or are a high Z' polymorphs, because of the high cost of the DFT-D calculations, or for a few free energy calculations because the algorithm failed. Optimization of MFA I from the different experimental starting points gave a lower energy than the global minimum, which was also a match for MFA I.

ID	Source of Structure			PBE0 _{intra} + FF _{inter} (kJ/mol)												Periodic DFT (kJ/mol)					
				ΔE_{intra}			CO Total			CO+FE			PCM Total			PBE+TS			PBE+MBD*		
	FFA	MFA	TFA	FFA	MFA	TFA	FFA	MFA	TFA	FFA	MFA	TFA	FFA	MFA	TFA	FFA	MFA	TFA	FFA	MFA	TFA
FFA I	E	M1971	P	4.34	5.12	7.00	3.37	12.35	8.32	3.13	11.71	7.87	3.34	12.62	4.77	3.82	4.60	8.25	3.64	4.70	11.18
FFA II	E	M1634	T158	2.00	4.39	0.97	-0.30	7.68	5.39	-0.33	7.17	6.39	0.30	10.04	5.84	0.45	8.11	2.30	5.62	9.69	8.10
FFA III	E	P	P	4.87	5.22	5.23	7.58	14.66	13.86	7.22	13.47		8.83	14.58	10.19	0.00	18.41	13.64	0.00	15.50	15.20
FFA IV	E			1.86			9.24			7.97			10.08		6.51			7.44			
FFA V	E			2.68			14.17						15.35								
FFA VI	E			10.25			21.33			19.65			22.72								
FFA VII	E			1.22			5.02			4.75			5.77		4.10			5.44			
MFA I	F1129	E	T917	3.23	2.57	2.07	11.60	-1.06	2.91	9.89	-1.53	2.21	10.83	0.66	2.39	10.69	0.00	8.31	7.75	0.00	6.49
MFA II _{Maj}	P	E	T7232	7.43	4.45	3.77	14.93	2.98	8.57	14.96	3.23	9.15	15.68	1.63	7.56		2.39	12.96		5.10	10.35
MFA II _{Min}	P	E	P	1.37	3.78	3.36	7.70	7.09	3.26	7.46	6.62		8.88	7.24	2.03		7.14	8.28		11.44	11.95
MFA III	P	E	T3074	2.26	3.56	3.08	16.34	3.90	3.73	16.17	3.42		18.24	2.81	2.62	20.13	-0.91	6.73	19.61	2.05	7.73
TFA I	P	M5643	E	4.50	3.59	2.34	10.26	5.80	2.42	10.53	5.46	2.28	9.53	5.06	0.67	17.30	3.96	6.22	9.20	3.67	3.42
TFA II	P	M2104	E	1.36	1.35	1.90	15.17	10.80	1.94	13.76		1.36	16.12	13.45	2.41	10.65	2.78	0.00	16.35	5.38	0.00
TFA III	F1248	M288	E	3.28	2.49	2.26	10.81	1.87	2.35	10.30	1.19	2.08	8.91	2.65	2.01	14.61	4.83	8.99	11.12	4.82	6.89
TFA IV			E		2.63	2.32		0.06	3.63		0.00	3.30								8.32	2.54
TFA Va	P	M497	E	7.39	4.80	3.74	14.93	7.08	8.58	14.89	6.64	8.92	15.73	7.02	7.59		10.10	8.28			6.93
TFA Vb			E		4.35	3.07		3.06	6.60		2.89	6.11		5.86				12.95			
TFA VIa	F1129	M128	E	3.23	2.63	2.03	11.60	0.06	2.91	9.89	0.00	1.75	10.83	0.00	2.33	10.69	-0.02	8.29	7.75		6.49
TFA VIb	F1129	M128	E	3.23	2.63	2.29	11.60	0.06	3.65	9.89	0.00	2.74	10.83	0.00	2.28	10.69	-0.02	8.27	7.75		6.28
TFA VII	F1173	M2853	E	3.08	2.45	2.49	11.32	2.74	6.91	10.26			10.03	3.05	5.11	12.10	6.91	7.89	9.16	5.04	7.72
TFA VIII	F1956	M510	E	3.31	4.29	2.39	9.15	2.49	3.01	8.49	2.61	2.80	8.22	1.85	1.13	11.22	4.77	8.14	13.09	6.22	5.55
FFA:TFA	E	M2853	E	2.14	2.45	2.49	10.50	2.74	6.91	9.48			10.07	3.05	5.11	12.10	6.91	7.89	9.16	5.04	7.72
FFA:MFA	E	E	T917	2.39	2.18	2.07	10.80	-1.33	2.91	9.28	-1.58	2.21	10.90	-0.17	2.39	10.69	0.00	8.31	7.75	0.00	6.49
MFA:TFA	F1129	E	E	3.08	2.15	2.08	11.32	-1.36	2.84	10.26	-1.44	2.34	10.83	-0.19	1.82	10.69	0.00	8.31	7.75	0.00	6.49

S4.1 Experimental rankings of crystal stability and assessment of accuracy of calculations

S4.1.1 MFA

For the case of MFA, SeethaLekshmi *et al*³ have performed crystallization, grinding and slurry experiments and note that under ambient conditions the stability order is I > II > III, whilst at higher temperature it is II > I > III. This order is corroborated by the work of Gilpin,¹⁷ in which the conversion of I to II was studied at temperatures between 150 and 160 °C. Hence, the lattice energies should give a stability order I > II > III. The disorder in MFA II means that its energy is somewhere between that of the major and minor component, which would be expected to be close.

The stability order of the experimentally observed MFA polymorphs with the force-fields is correct, with MFA I > MFA II major > MFA III > MFA II minor. The force field calculations agree better with the observed metastability of MFA III than the periodic DFT-D calculations. All methods give a difference of about 5 kJ/mol between MFA II major and MFA II minor, which is rather larger than would suggest disorder. The contrast between the PBE-TS and when the dispersion is replaced by MBD* emphasizes the sensitivity of the MFA relative stability to dispersion. This is consistent with the contribution of $\pi \cdots \pi$ interactions in the stabilization of II and III being much greater than in I, as

the twisted, lower energy conformation ($\phi=64^\circ$) in MFA I hinders $\pi\cdots\pi$ stacking relative to the more perpendicular aromatic rings ($100^\circ < \phi < 110^\circ$) of I and III.³

S4.1.2 TFA

Lopez-Mejias *et al*⁵ performed DSC experiments on TFA, giving the order (ΔH_{fus} , T_{melt}) to be III (41.80 kJ/mol; 214.09 °C), V (41.63 kJ/mol; 215.17 °C), I (39.37 kJ/mol; 213.10 °C), II (38.70 kJ/mol; 213.52 °C), IV (31.88 kJ/mol; 206.78 °C), although III and V transform before melting, and work by Mattei suggests that II may transform to I before its melting temperature.¹⁸ Thus Lopez-Mejias *et al*⁵ show that III, IV and V are metastable polymorphs, but are inconclusive about the relationship between forms I and II. From optical absorbance experiments in iso-octane, the $\Delta\Delta G$ (kJ/mol) ordering was I (0.00), II (0.17), III (0.42), V (0.96), IV (1.13). On the other hand, earlier ΔH_{fus} measurements have form II to be approximately 6 kJ/mol more stable than form I,⁴ however Surov deduced a monotropic relationship with form I more stable than form II and no heat events observed in a DSC before melting.¹⁹ Mattei¹⁸ observes that II converts to I in slurry at 25 °C and in the DSC at 141.8 °C, concluding that form I is the more stable form from room temperature until melting. They observe from the DSC that the II to I conversion is endothermic. Another contradictory report is the observance by Gilpin of form I converting to II between temperatures of 90 and 100 °C.¹⁷ From these three studies^{4, 18, 19} we take TFA II to be more stable than TFA I at 0 K²⁰ and therefore the order of stability for lattice energies should be $\text{II} \geq \text{I} > \text{III}, \text{IV}, \text{V}$, although TFA I was used as a template crystal as it is the stable form at room and high temperature. It is noted, though, that the evidence as to the relative stability of forms I and II at the zero kelvin limit is not clear, but our designation of form II being lower in lattice energy is only to help understand theoretical rankings and will not change the conclusions of this paper.

The crystal energy landscape (PCM) has all TFA polymorphs, except disordered TFA V, within 2 kJ/mol in stability order $\text{TFA I} > \text{VII} > \text{III} > \text{VI} > \text{II} > \text{IV} > \text{V}$. The periodic DFT and the CrystalOptimizer model have TFA II more stable than TFA I, with the periodic DFT giving a larger spread of energies, though the order depends on the dispersion model. It is clear that the TFA polymorphs are not well separated in energy in either the computational or experimental measurements. The new polymorphs are calculated to be metastable.

S4.1.3 FFA

For FFA, the experimental data on enthalpy and temperature of fusion (ΔH_{fus} ; T_{fus}) from DSC measurements⁷ is form III (29.7 kJ/mol; 127.4 °C), I (27.6 kJ/mol; 134.5 °C), V (25.5 kJ/mol; 124.9 °C), II (24.7 kJ/mol; 129.6 °C), VI (24.7 kJ/mol; 124.2 °C), VII (23.4 kJ/mol; 120.7 °C), IV (22.6 kJ/mol; 123.9 °C),⁷ and $\Delta\Delta G$ from optical absorbance in water at 27 °C (kJ/mol) III (0.00), I (0.17), II (0.46), IV (0.71), VI (0.75), VII (1.05).⁷ Forms I, II and III all melt without passing through another form, but the DSC is more complicated for IV-VII. Of I-III, form III has the largest ΔH_{fus} and the lowest T_{melt} , which Burger and Ramberger's heat of fusion rule associates with enantiotropic phase changes to the other forms. Form I on the other hand has both a higher ΔH_{fus} and T_{melt} than form II, which would imply a monotropic relationship between this pair. Studies of phase changes in FFA show that III transforms to I on heating at 42 °C,²¹ and these are the most stable forms over the range of experimentally relevant temperatures, with form II appearing to be metastable. Hence, the low temperature stability order is $\text{III} > \text{I} > \text{II}$, with the other forms probably being even more metastable.

The most significant difference between the lattice energy calculations (which approximate conditions at 0 K) and experimental observations, is that FFA III is known to be the polymorph which is most stable at room temperature. The atomistic modelling calculations of the CSP study predict FFA III to be significantly less stable than FFA I or II. This appears to be due to the empirical

exp-6 fluorine repulsion being too repulsive, as III and V have direct $\text{CF}_3 \cdots \text{F}_3\text{C}$ interactions (motifs 5a and 6aγ in Figure S2) which appear to be destabilizing them relative to other polymorphs. The periodic *ab initio* at PBE-TS, PBE-D02 (not shown) and PBE-TS/MBD* level all give polymorph FFA III as the most stable structure. The relative stability of the other polymorphs varies significantly with dispersion correction, changing the stability of FFA II relative to FFA III by around 5 kJ/mol.

S4.1.4 Overall comparisons of energies

The estimates of relative stability are limited by the neglect of free energy contributions which could produce significant reranking, given that an enantiotropic phase change is observed for all three molecules. The rigid-molecule harmonic free energy estimates in Table S10 only partially change the stability order, but, as noted for MFA I above, the libration of the aromatic ring is likely to make a substantial polymorph specific contribution to the free energy. The relative lattice energies, even at the PBE-MBD* level, may well be in error from the dispersion model, and may suffer from the use of a functional (PBE) that gives a poorer description of the molecular properties than that used in the CSP study (PBE0). The MBD* van der Waal's energy correction is a better model for the dispersion than the TS model, and the periodic PBE-TS calculations have some obvious errors in relative stability: giving MFA III to be more stable than MFA I, and FFA II to more stable than FFA I; and of most concern that TFA II is 6.2 kJ/mol lower in E_{latt} than TFA I. The empirical potentials have considerable limitations, and in this case the $\text{F} \cdots \text{F}$ model destabilizes FFA III significantly. However, this error, whilst giving a poor crystal energy landscape for FFA, appears to only affect the structures with the $\text{CF}_3 \cdots \text{F}_3\text{C}$ interaction specific to FFA III and is not so large as to invalidate the finding of isomorphous structures in this series.

The periodic PBE-MBD* would be expected to be the most theoretically accurate, currently affordable method for this type of molecular crystal. It correctly predicts that MFA I, TFA II, and FFA III are the most stable forms by E_{latt} , in agreement with the observed stability at low temperature, and therefore these energies are in Figure 6 of the manuscript.

Taking the set of structures calculated by the different methods together (Table S10), and within the uncertainties of the different weaknesses of the methods, we note:

- (1) The low energy forms MFA I, TFA II, and FFA III are calculated to be the lowest energy at low temperatures.
- (2) No isomorphous structure identified by comparison of the crystal energy landscapes (Table S9) is more stable than the known forms. Hence, the templating experiments could only target metastable forms.
- (3) The energy range of the observed ordered polymorphs is reasonable, given that ΔE_{latt} , calculated by a similar force field to ours, did not exceed 7.2 kJ/mol for 95% of pairs of polymorphs in a test set of 1061 structures for 508 molecules,¹⁵ and periodic PBE-D02 calculations gave 90% of polymorphs differing by less than 4 kJ/mol for 446 structures of 215 smaller molecules.²²
- (4) The disordered polymorph MFA II consistently has a rather high energy for the minor component, and the difference in energy between the TFA V disorder components varies with method. This may be due to the limitations of deducing ordered models from the crystallographic data. The new disordered polymorph TFA VI has both components close in energy.
- (5) The new polymorphs TFA VI, TFA VII and TFA VIII are within the energy range of the previously known polymorphs, with TFA VI being close in energy to the similar TFA IV.

- (6) The solid solution MFA:TFA \sim MFA I which covers the entire range has similar energies for both MFA and TFA. In contrast the solid solutions with FFA which do not go to pure FFA end-points have much higher energies for the hypothetical pure FFA than the TFA endpoint that was found (TFA VII).
- (7) The energy difference between TFA VI (\sim MFA I) and TFA VII (\sim TFA:FFA) is small and depends on the dispersion correction, which is not surprising since they have a coordination cluster of 12 molecules in common (Figure S7). The difference between the corresponding MFA structures is larger, (5.04 kJ/mol at PBE-MBD*), though this is similar to the metastability of TFA VI and TFA VII relative to TFA's most stable form TFA II. It is observed in this work that TFA can be sublimed onto MFA I or TFA:FFA, and yield TFA VI and TFA VII respectively, whilst MFA will only take the structure of MFA I. This strongly suggests that there is no clear cutoff in terms of thermodynamic metastability for the observation of polymorphs, and their formation by templating depends on the effect of the surface in catalysing the nucleation and preventing the transformation to the most stable form.

Generally each molecule is relatively more stable in its own known structures than in those observed for another molecule. This is particularly marked for FFA, which is consistent with not finding more polymorphs of this highly polymorphic system. The force field and periodic DFT methods predict similar energy differences with regards to the questions that we are trying to answer in this paper, which gives us confidence in using force-fields to survey the landscape, and DFT to make more precise comparisons.

S5. Nanocrystal surface docking calculations

In order to characterize and quantify interactions at the surfaces which are relevant to the templating experiments, modelling work has been performed on the two solid solution structures. A nanocrystal of one material was docked onto the surface of another, in order to measure the strength of interactions which would be found across the surface, and to test the registry of the surface topologies.

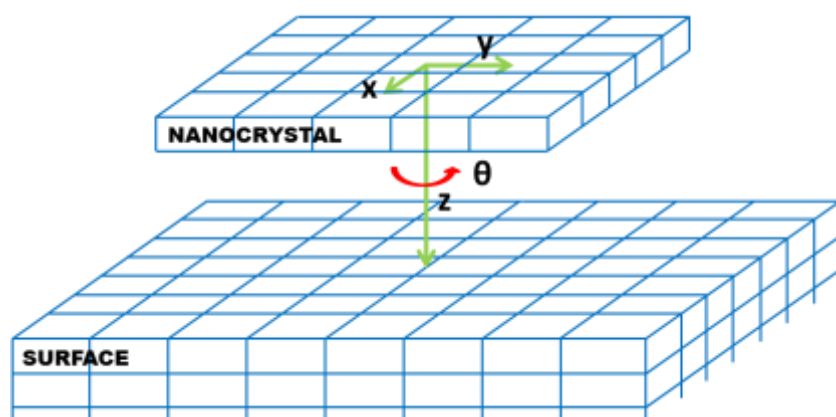


Figure S8. Schematic of the docking calculation. The 5x5 molecule nanocrystal was orientated at the angle θ so as to make the best continuation of the lattice possible, as described in the text. The translational degrees of freedom, x, y and z, are optimized by ORIENT.²³

S5.1 Methodology

Both solid solution structures (isostructural with MFA I (P-1) and TFA VII (P₂₁/c)) in the limit of a pure (Z'=1) composition of each of the three molecules, were minimized with CrystalOptimizer and single point energies calculated with DMACRYS with a PCM model. These optimized structures, are the ones that were used in the bulk lattice energy analysis in Table S10. A cut was prepared so that docking was considered at the dominant face of the crystal: this is (100) for the P-1 structure, and (010) face for P₂₁/c (Figure S12 and Figure S25 respectively). There is a significant variation in the surface cell dimensions between the different molecules (Table S11) which depends on crystal structure as well as the molecular change. The addition of another layer to this surface was modelled by preparing a 25 molecule nanocrystal (5x5) from these same PCM optimized structures.

Table S11. Structural parameters for surfaces used in the docking experiments.

	a' /Å	b' /Å	γ'/° (sin(γ'))	a'.b'.sin(γ')/Å ²
MFA (P-1)	6.94	7.36	115.37 (0.90)	46.15
TFA (P-1)	6.91	7.29	115.14 (0.91)	45.60
FFA (P-1)	6.56	7.31	111.68 (0.93)	44.56
MFA (P ₂ ₁ /c)	7.00	7.72	123.22 (0.84)	45.21
TFA (P ₂ ₁ /c)	6.85	7.57	126.34 (0.81)	41.77
FFA (P ₂ ₁ /c)	7.35	7.88	129.49 (0.77)	44.70

The starting position of the nanocrystal was parallel to the infinite surface at z=3.5 Å above the crystallographic position, with θ chosen such that if the nanocrystal and the surface were from the same structure (a 5x5 nanocrystal of MFA I attaching to the MFA I surface, for example) the nanocrystal would simply be a continuation of the surface crystal structure. Hetero-surfaces were also prepared, and the orientation of the nanocrystal was chosen to minimize the RMSD between the non-acidic ring of the nanocrystal and that of the lowest molecule in the surface unit cell, i.e. that which it would be related to by translation in the case in which the nanocrystal was a continuation of the surface structure. The position of the nanocrystal relative to the surface was optimized by varying x, y and z only, as it was not possible to vary θ without also varying the other variables defining the orientation of the nanocrystal. In cases in which the isostructurality of the structures used to make the surface and the nanocrystal was not very high, it is not possible to find a value of θ which allowed even this small nanocrystal to dock well.

The translational degrees of freedom of the nanocrystal were optimized with the same force field as has been used in the lattice energy optimizations, with the program ORIENT,²³ and interaction energies are given per mole of nanocrystal, i.e. divided by 25 for the 5x5 nanocrystals. Interactions were summed to a large cutoff of 60 Å.

S5.2 Docking Results

Table S12. Interaction energies, $U_{\text{interNano}}$, per molecule of nanocrystal. All energies in kJ/mol (of nanocrystal).

nano \ surface	MFA (P-1)	TFA (P-1)	FFA (P-1)	MFA (P2 ₁ /c)	TFA (P2 ₁ /c)	FFA (P2 ₁ /c)
MFA (P-1)	-61.84	-46.82	-19.72	-17.30	-15.18	-11.16
TFA (P-1)	-68.88	-47.68	-14.15	-18.43	-9.00	-11.56
FFA (P-1)	-19.08	-23.06	-43.19	-10.51	-9.79	-7.85
MFA (P2 ₁ /c)	-14.56	-13.81	-8.83	-41.04	-27.91	-14.50
TFA (P2 ₁ /c)	-14.37	-15.02	-8.11	-31.16	-37.88	-15.32
FFA (P2 ₁ /c)	-9.56	-12.20	-8.54	-14.13	-21.20	-53.19

The three molecules, in two structural forms, can be used to make six nanocrystals docked onto six surfaces. The $U_{\text{interNano}}$ matrix (SI Table S12) is clearly in block diagonal form: docking of P-1 nanocrystals onto P2₁/c surfaces, and vice versa, leads to much weaker interaction energies than using the same 2D lattice reflecting the difference in surface unit cells (Table S11). Even when the nanocrystal and surface are from the same structural type, there are marked differences with the constituent molecules. FFA does not dock well with other molecules, although TFA and MFA are more compatible with each other. The strongest interaction in the set is for the TFA P-1 nanocrystal docking on an MFA P-1 surface (-68.9 kJ/mol), which corresponds to the experiment which caused the templating of TFA VI.

The block of P2₁/c nanocrystals and surfaces generally shows less strong interactions than their P-1 equivalents, particularly for MFA and TFA which have two substituent groups which achieve a favourable “broadside” configuration across the surface in the P-1 docking case. The effect is strongest for MFA, which has been seen experimentally to always favour the P-1 over P2₁/c structure in templating experiments.

The behaviour of FFA shows stronger docking for the P2₁/c nanocrystal on the P2₁/c surface than is seen in the P-1 structures. FFA has one non-hydrogen substituent on the non-acidic ring, which will decrease the van der Waals interactions in the 6a configuration of Figure S2, but the CF₃ group is in the meta position and still in contact with the ring of its neighbour (6aβ interaction). The weakest interactions in the set often involve FFA P-1. The reason for this is the sizable relaxation of the FFA P-1 structure from the MFA I structure starting point, which is caused by the lack of interactions from the missing ortho group of the non-acidic ring. There is also a component from the different intramolecular PES (Figure S3) for this molecule when compared to MFA and TFA, with FFA preferring smaller ϕ angles. This change in the FFA P-1 structure leads to visibly different surface interactions with the rigid modelling presented here, as is seen in Figure S9.

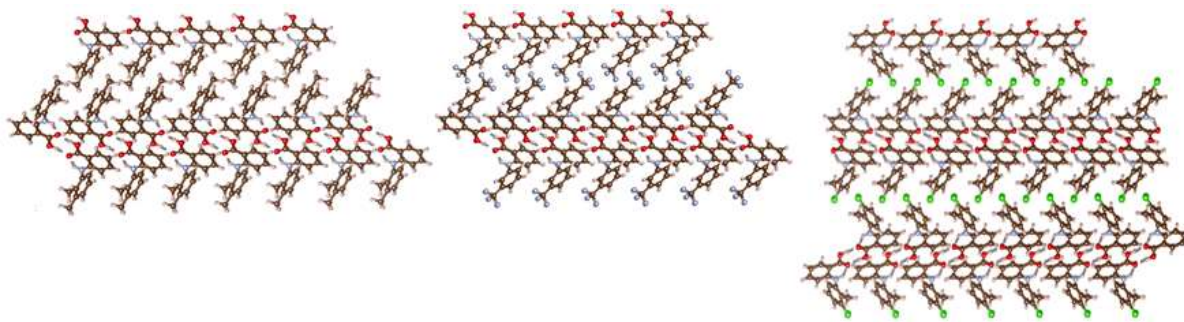


Figure S9. Examples of docking final structures, with the same molecule and structure used for both the nanocrystal and surface. From left to right: MFA I (P-1), which shows the nanocrystal penetrating the surface and therefore a strong interaction; FFA (P-1) in which the relaxation of the bulk cell leads to a surface interaction without penetration and an attenuated interaction; TFA VII (P21/c), which has a similar surface, but the screw axis leads to different layers of hydrogen bonded dimers beneath and above the surface, with T-interactions (type 6a β in Figure S2) which are generally less strong than the broadside interactions of P-1 (type 6a).

Any realistic reproduction of the processes occurring at the template surface would sample a very wide range of configurations of the system, rather than the rigid nanocrystal docking presented here. The lack of relaxation within the surface or the nanocrystal, (or variation of θ during the optimization) has resulted in a large difference in energies for cases of good versus poor docking, as the exponential repulsion exaggerates the energy differences for slight mismatches. Nevertheless, these calculations agree with the experimental results, notably in that TFA is a natural and strong fit at both dominant surfaces, and so the template could steer the TFA molecules into the novel forms VI and VII.

S6. Solution templating of TFA VI from FFA I

Crystallizing TFA from ethanol was found to be affected by seed crystals of FFA, with FFA I leading to the observance of the new form TFA VI, whereas FFA III did not. FFA III is unlikely to act as a seed for any polymorph of TFA or MFA, as there is a large energy penalty to force these molecules into the high dihedral angle (Figure S3). The structure of TFA VI is, however, a partial match to that of FFA I. When overlaying a cluster of 15 molecules, 5 match with an RMSD of 0.242 Å.

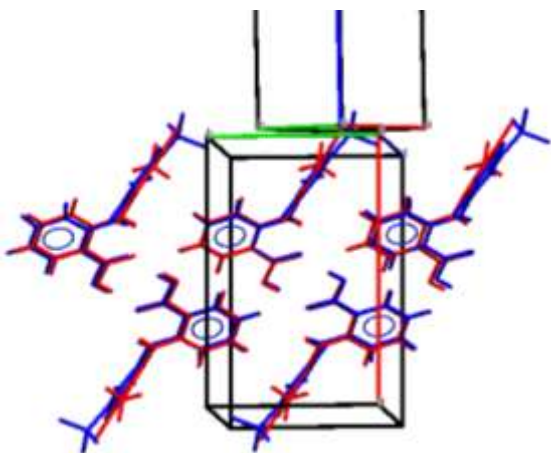


Figure S10. Overlay of 5 molecules of FFA I (blue) and TFA VI (red). The unit cells are also drawn, and it is noted that the *a* axis (red) of FFA I (lower unit cell) is roughly aligned with the *c* axis of TFA VI (blue, upper unit cell).

S7. Crystallization and powder XRD data

All the materials used in the work, mefenamic acid, tolfenamic acid and flufenamic acid were obtained from Sigma-Aldrich and were used as received.

Powder X-ray diffraction data collection of the material obtained from crystallization experiments was carried out on a Bruker D8 Discover diffractometer, operating in reflection geometry, with Cu K α radiation ($\lambda=1.5418$ Å), fitted with a Divergent slit and a LynxEye linear detector. Data for all the samples were collected over the angular range $4 \leq 2\theta / ^\circ \leq 40$, using counting time of 1 sec/0.01° increments of detector position. Pawley refinements were carried out on TOPAS 5.0.²⁴

S7.1 Powder X-ray diffraction

S7.1.1 Crystallization of TFA VI

Template Preparation: Single crystals of MFA I were obtained by slow evaporation at room temperature from ethanolic solution of MFA. The resulting material was analyzed by powder X-ray diffraction and was found to be pure MFA I (Figure S11). Face indexing of MFA I single crystals (Figure S12) indicates that (100) is the dominant face of MFA I crystals.

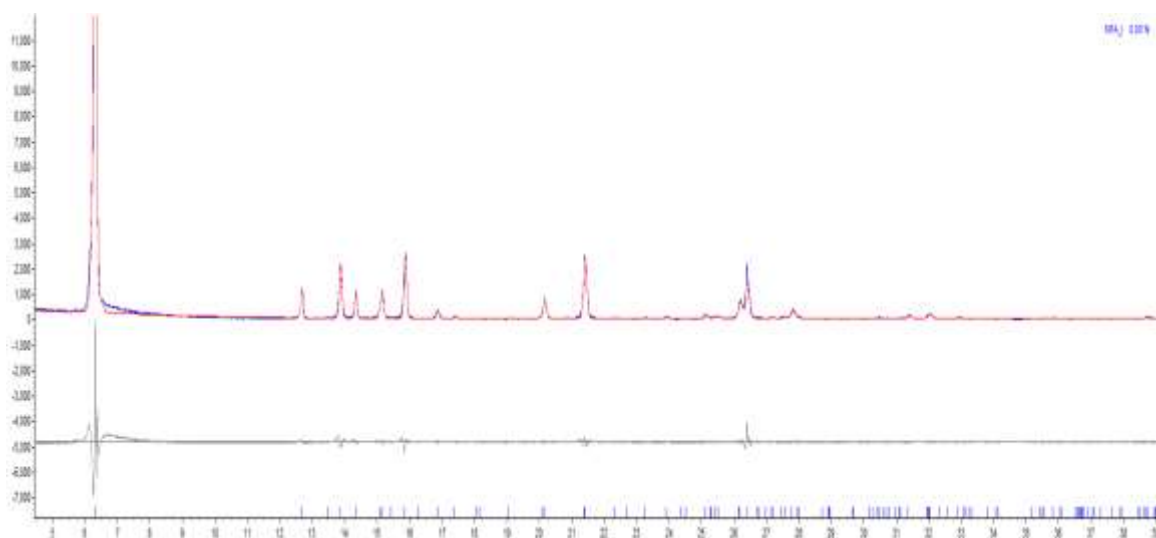


Figure S11. Pawley-type fit of MFA obtained by recrystallization from ethanol solution. The refined unit cell parameters are: $[a=14.587(6)$ Å, $b=6.812(7)$ Å, $c=7.672(3)$ Å, $\alpha=119.61(2)^\circ$, $\beta=104.96(3)^\circ$, $\gamma=91.4(2)^\circ]$. The final residual values are $R_p=8.8\%$ and $R_{wp}=12.62\%$.

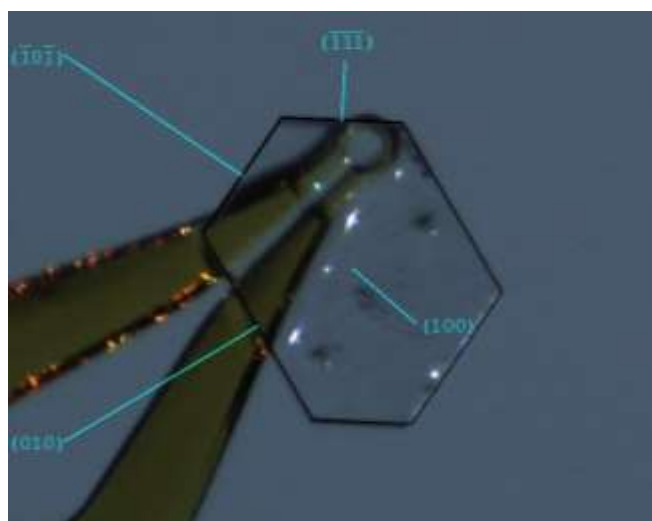


Figure S12. Face indexing of MFA I.

An array of MFA I single crystals were mounted on a glass slide and used as substrates for the vapour deposition of TFA. Around 40 mg of TFA was placed in a petri dish which was then placed on a heating plate held at 120 °C. The glass slide upon which the array of single crystals was mounted was placed on top of the petri dish and the templates exposed to TFA vapours for ~ 24 hrs. The resulting TFA crystals that were deposited on the MFA I surface were analyzed by optical microscopy (Figure S13) and single crystal X-ray diffraction (Table S17).



Figure S13. TFA deposited MFA I crystals.

S7.1.2 Crystallization of TFA VI from solution by seeding

Hetero-seeding experiments were performed to test this route to new forms. MFA form I seeds were obtained by recrystallization of MFA from acetonitrile by room temperature solvent evaporation to dryness. Several small MFA I seeds were transferred to a saturated solution of TFA in ethanol. After room temperature evaporation of the TFA ethanol solution to dryness, clusters of single crystals with a block morphology were observed and were separated and analyzed by SCXRD to give the structure of TFA VI, as described in Section S7.2 and Table S17.

TFA VI crystals can also be obtained by seeding a saturated ethanolic solution of TFA with a couple of FFA I crystals. Pawley profile fitting of the material whilst using TFA VI unit cell parameters indicate good agreement between the calculated and experimental pattern (Figure S14).

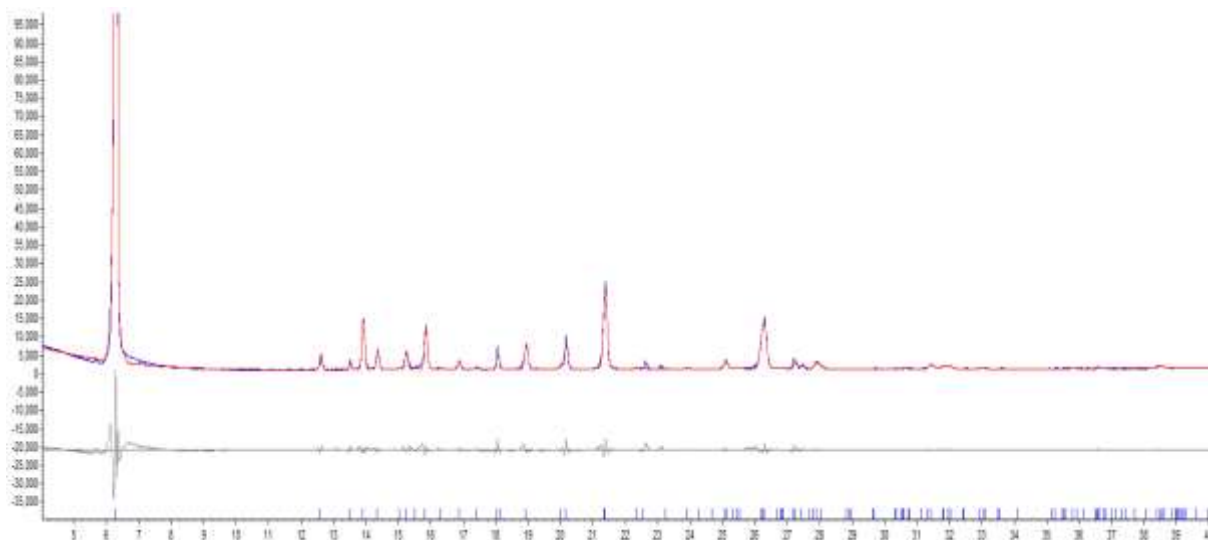


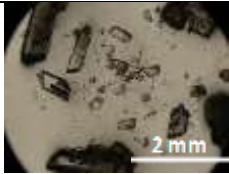
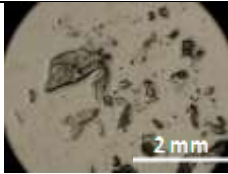
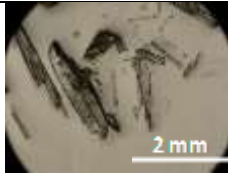
Figure S14. Pawley fit of material obtained by seeding TFA solution with FFA I crystals. The material is predominantly TFA VI. The refined unit cell parameters are: [$a=6.799(5)$ Å, $b=7.284(6)$ Å, $c=14.523(3)$ Å, $\alpha=76.86(3)^\circ$, $\beta=79.04(4)^\circ$, $\gamma=65.95(7)^\circ$]. The final residual values are $R_p=6.20\%$ and $R_{wp}=10.3\%$.

S7.1.3 Co-crystallization of MFA:TFA solid solution

Co-crystallization experiments were carried out by solvent evaporation to dryness at room temperature from ethanol, di-ethyl ether and acetonitrile. The molar ratios of MFA:TFA used in each solvent were 50:50, 40:60, 30:70, and 20:80 (reported as mole fraction of TFA=0.5, 0.6, 0.7, 0.8). Colourless block crystals were obtained after a few days and displayed crystal morphologies that were similar to that of MFA form I. Crystals obtained from ethanol were used for SCXRD (Table S13). The bulk material was tested by DSC to confirm only a single melting event was observed, *i.e.* to confirm that there was no significant amount of the pure starting components present, and then tested by NMR for composition.

Single crystal X-ray diffraction data for TFA VI and MFA:TFA solid solutions were collected at 150 K using an Agilent SuperNova diffractometer, equipped with an Oxford Instruments Cryojet5 and Cu-K α radiation ($\lambda=1.54184$ Å). Structures were solved with SHELXS and refined with SHELXL within the Olex2 GUI. The relative MFA:TFA ratio in the experimental solid solution crystals was determined by refining the site occupancy of the CH₃ and Cl groups.

Table S13. The observed morphologies and crystallographic data of the crystals in the MFA:TFA solid solution series. *Low quality data, structure not reported in full.

Solution mole fraction of TFA	0.5	0.6	0.7*	0.8
				
a (Å)	6.7312(9)	6.7336(4)	6.7295(16)	6.7241(8)
b (Å)	7.2896(10)	7.2720(4)	7.2619(15)	7.2432(8)
c (Å)	14.2268(15)	14.2713(10)	14.269(4)	14.3139(15)
α (°)	77.197(10)	77.150(5)	77.25(2)	77.181(9)
β (°)	79.624(10)	79.547(6)	79.59(2)	79.411(10)
γ (°)	65.533(13)	65.678(6)	65.74(2)	65.937(11)
Cell Volume (Å ³)	616.52(15)	617.66(7)	616.9(3)	617.27(13)
R1 (I > 2 σ (I))	0.0737	0.0609	0.0937	0.0710
R factor (all)	0.0981	0.0690	0.2355	0.0832
Mole fraction of TFA by SCXRD refinement	0.43(1)	0.58(1)	0.64(1)	0.78(1)

S7.1.4 ¹H NMR of MFA:TFA solid solutions

¹H NMR spectra were collected on CDCl₃ solutions of the MFA:TFA solid solution series, as well as for commercial MFA and commercial TFA on a Bruker Advance 300 MHz NMR spectrometer operating at room temperature. Integration of the ¹H NMR spectra was used to determine the mole fraction of TFA present in the bulk solid solution crystals. The corroboration between NMR and PXRD for MFA:TFA concentrations is shown in Table S14.

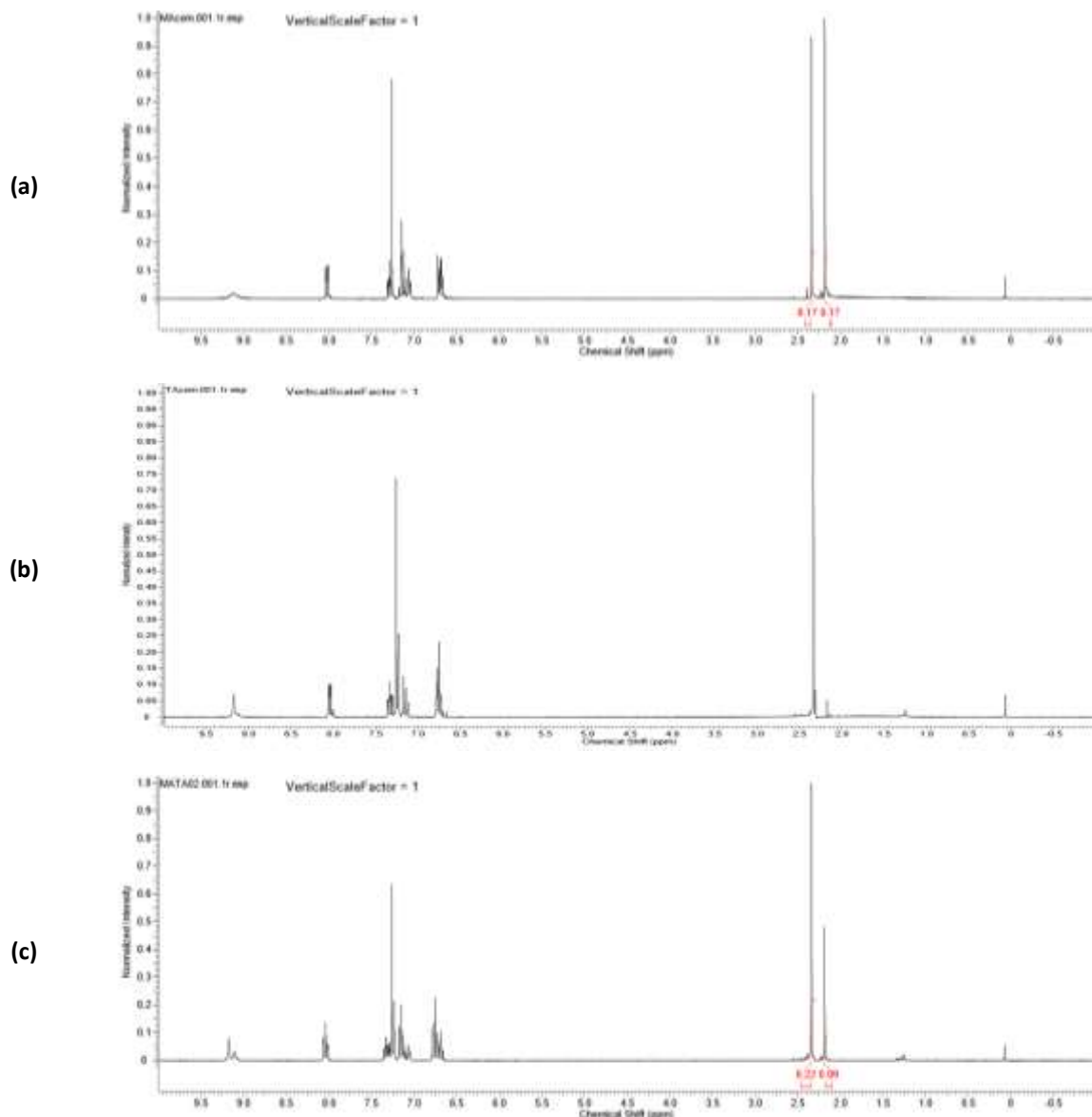


Figure S15. ^1H NMR spectra of (a) commercial MFA, (b) commercial TFA and (c) a MFA:TFA solid solution (target mole fraction of TFA is 0.6).

Figure S15 shows the ^1H NMR spectra for commercial MFA which has two peaks, of equal integral, at 2.34 ppm and 2.18 ppm arising from the presence of two methyl groups on the MFA molecule. In comparison, 14b shows the ^1H NMR spectra of commercial TFA which has only one peak at 2.34 ppm as the TFA molecule has only one methyl group. Figure 14c shows the ^1H NMR spectrum for the target 0.6 mole fraction of TFA which has two peaks that differ in integral, at 2.34 ppm and 2.18 ppm. The content of TFA in each solid solution crystal can be determined by integration of the peaks at 2.34 ppm and 2.18 ppm against each other, noting that the 2.18 ppm peak is only present due to MFA in the solid solution crystals while the peak at 2.34 ppm contains contributions from both components.

Table S14. The mole fractions of TFA present in the MFA:TFA solid solution series from ^1H NMR spectroscopy.

Target mole fraction of TFA	0.5	0.6	0.7	0.8
SCXRD	0.43(1)	0.58(1)	0.64(1)	0.78(1)
Mole fraction of TFA from integration of ^1H NMR spectra	0.43	0.60	0.69	0.76

Given the quality of the crystallographic data, the two sets of data are self-consistent and do not deviate significantly from the solution phase ratios of MFA and TFA.

S7.1.5 Co-crystallization of equimolar amounts of MFA and FFA from solution
Crystallization of equimolar amounts of MFA and FFA from ethanoic solution resulted in the crystallization of material containing predominantly MFA I and FFA II as shown in Figure S16.

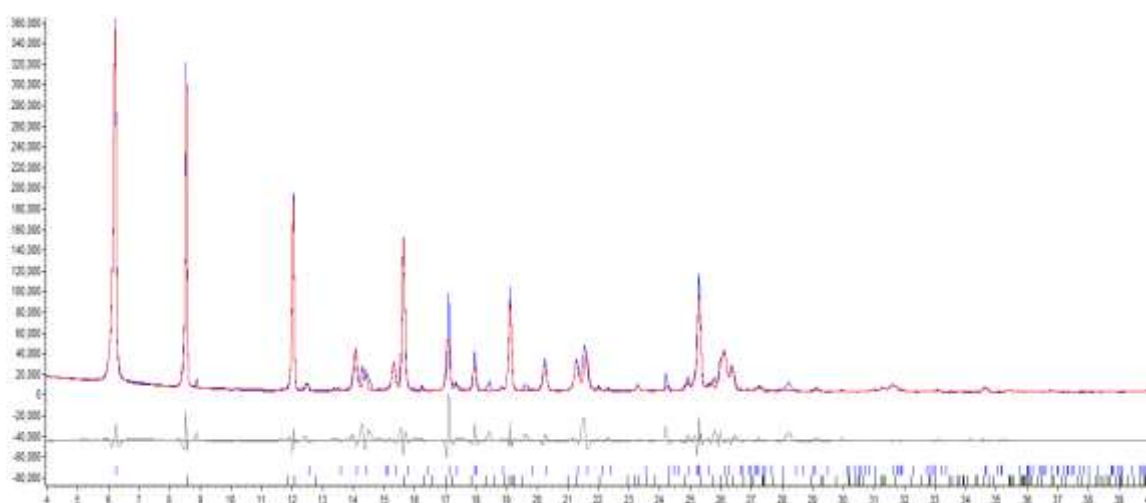


Figure S16. Pawley fit of material obtained by crystallization from solution using equimolar amounts of MFA and FFA. MFA I (blue reflections) and FFA II (black reflections) unit cell parameters. The refined cell parameters of MFA are: [$a=14.787(2)$ Å, $b=6.823(4)$ Å, $c=7.566(3)$ Å, $\alpha=119.57(2)^\circ$, $\beta=104.87(2)^\circ$, $\gamma=90.97(3)^\circ$] and for FFA II are: [$a=11.011(3)$ Å, $b=10.420(7)$ Å, $c=11.461(2)$ Å, $\alpha=90.0^\circ$, $\beta=111.03(4)^\circ$, $\gamma=90.0^\circ$]. The residual values from the Pawley fit are $R_p=11.26\%$ and $R_{wp}=17.60\%$.

S7.1.6 Crystallization of MFA:FFA solid solution from melt.

Since crystallization of MFA and FFA alone from solution only resulted in known polymorphs of MFA and FFA. Crystallization from the melt was attempted, where in finely ground molar ratios of MFA:FFA in 80:20, 30:70 were placed between two glass slides and the material melted on a Kofler bench by heating to 175 ± 5 °C. The material was then allowed to cool to RT slowly by decreasing the temperature at 5 °C/min. The resulting solid materials was analyzed by powder, to confirm that the material had not decomposed and single crystal X-ray diffraction. The results are summarized in Table S15.

Table S15. Summary of MFA:FFA crystallization from melt.

Molar amounts of MFA:FFA	Crystallization outcome by PXRD.
80:20	Predominantly MFA II
30:70	(FFA) _{0.7} :(MFA) _{0.3} solid solution

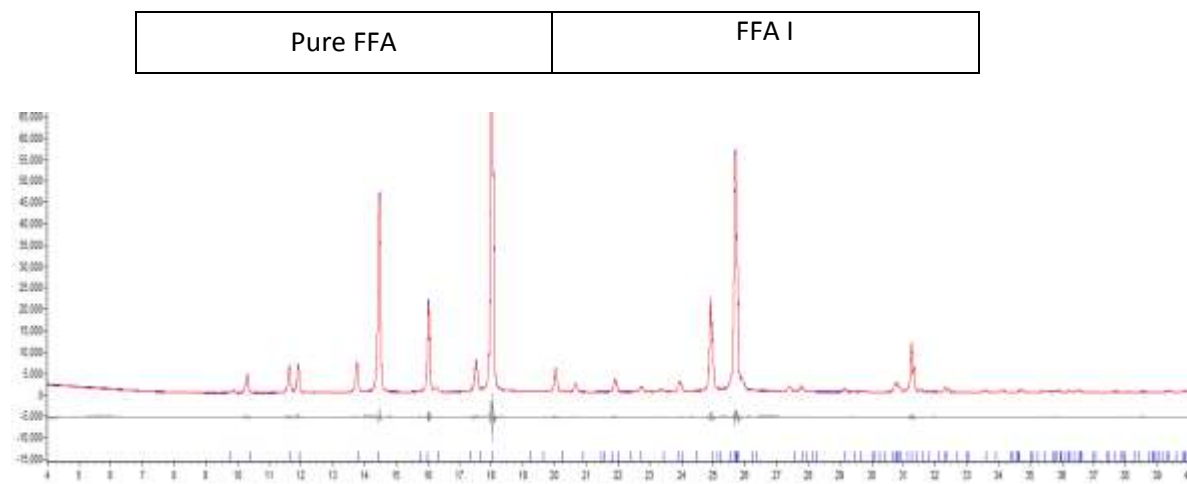


Figure S17. Pawley fitting of material obtained by crystallization from melt of MFA:FFA (80:20) material, the material was predominantly MFA II. The unit cell parameters after Pawley fit are: [$a=7.814(4)$ Å, $b=9.123(7)$ Å, $c=9.443(5)$ Å, $\alpha=106.69(3)^\circ$, $\beta=92.29(5)^\circ$, $\gamma=101.38(6)^\circ$]. The residual values after Pawley fit are $R_p=8.8\%$ and $R_{wp}=12.03\%$.

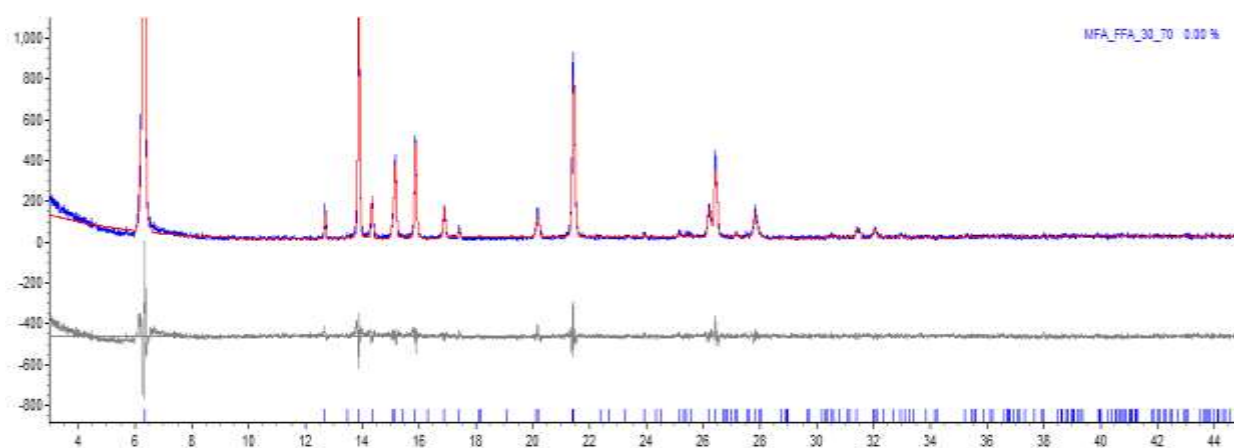


Figure S18. Pawley fitting of material obtained by crystallization from melt of MFA:FFA (30:70) material, the material was predominantly MFA:FFA solid solution. The unit cell parameters after Pawley fit are: [$a=6.708(4)$ Å, $b=7.228(7)$ Å, $c=15.410(5)$ Å, $\alpha=78.28(3)^\circ$, $\beta=77.62(5)^\circ$, $\gamma=66.68(4)^\circ$]. The residual values after Pawley fit are $R_p=12.38\%$ and $R_{wp}=14.03\%$.

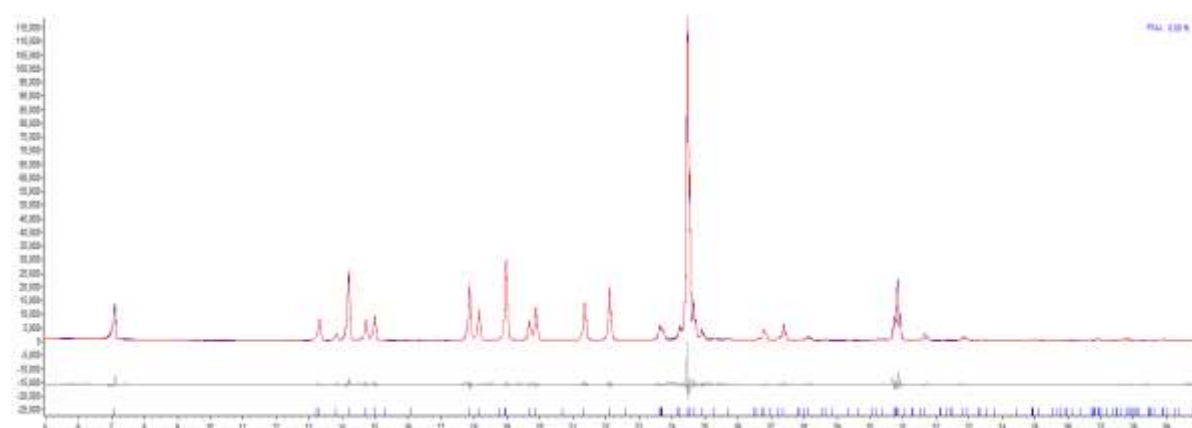


Figure S19. Material obtained when FFA was crystallized from the melt. The material matches with that of FFA I. The refined unit cell parameters are: [$a=12.534(4)$ Å, $b=7.862(3)$ Å, $c=12.868(5)$ Å, $\alpha=90.0^\circ$, $\beta=94.96(3)^\circ$, $\gamma=90.0^\circ$]. The residual values after Pawley fit are $R_p=7.01\%$ and $R_{wp}=9.98\%$.

S7.1.7 Seeding the melt of FFA with MFA:FFA single crystal

Upon heating, at ~ 150 °C, FFA III material turns into a melt. Seeding the melt of FFA III with single crystals of MFA:FFA solid solution followed by slow cooling of the material to RT at 5 °C per minute results in a material that is predominantly a mixture of FFA I and FFA III (Figure S20).

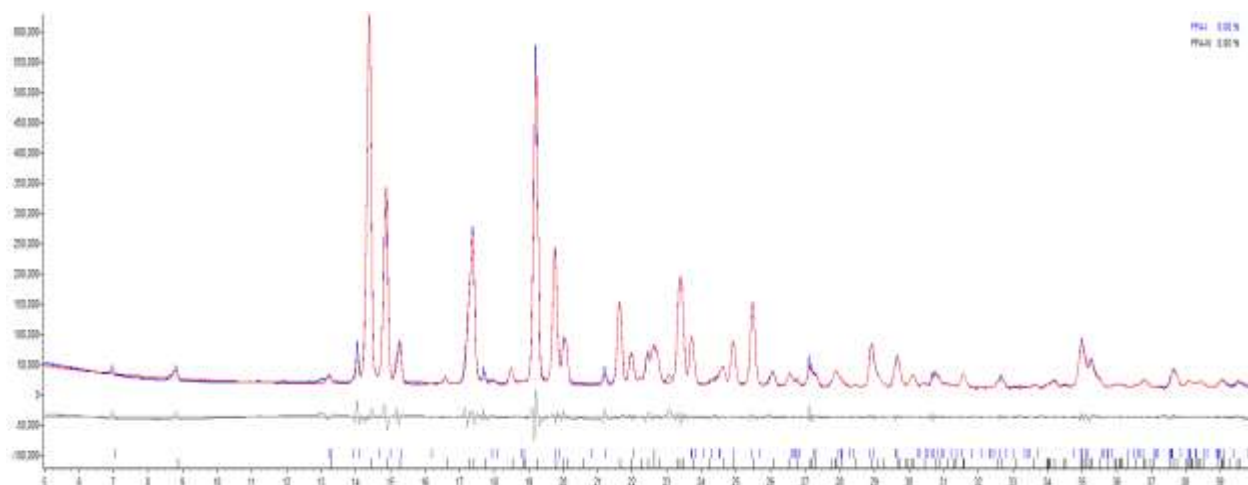


Figure S20. Pawley fitting of material obtained by seeding FFA III melt with MFA:FFA solid solution, using unit cell parameters of FFA I (blue) and FFA III (black). The refined cell parameters of FFA I are: [$a=12.632(5)$ Å, $b=7.883(1)$ Å, $c=12.842(5)$ Å, $\alpha=90.0^\circ$, $\beta=96.21(4)^\circ$, $\gamma=90.0^\circ$] and for FFA III are: [$a=39.966(1)$ Å, $b=5.126(9)$ Å, $c=12.267(4)$ Å, $\alpha=90.0^\circ$, $\beta=92.504(1)^\circ$, $\gamma=90.0^\circ$]. The residual values after Pawley fit are $R_p=5.23\%$ and $R_{wp}=7.32\%$.

S7.1.8 Co-crystallization of TFA:FFA solid solutions

Varying molar amounts of TFA:FFA were dissolved in ethanol and the material allowed to crystallize by slow evaporation at room temperature. The input molar amounts of TFA:FFA were 20:80, 50:50, 60:40, 80:20. The resulting bulk materials from the crystallization experiments were analyzed by powder and single crystal X-ray diffraction. Whilst the bulk powder data is consistent with the single crystal X-ray diffraction data in 50:50 and 60:40 solid solutions, other crystallization experiments resulted in concomitant crystallization of other known polymorphs of TFA and FFA alongside single crystals of solid solutions with varying amounts of TFA:FFA. Importantly FFA V crystals can be readily obtained from ethanolic solution of TFA:FFA in 20:80 mole ratio. After analysis of a number of single crystals, we observe that the maximum amount of TFA and FFA in the solid solution crystals goes up to ~ 70 and 50 % respectively from solution based crystallization experiments. Table S16 summarizes the results from solid solution experiments.

Table S16. Summary of TFA:FFA solid solution experiments.

Molar ratios of TFA:FFA in solution	PXRD analysis of bulk material	SCXRD analysis of single crystals
20:80	Predominantly FFA V	FFA V and TFA:FFA in 50:50 mole ratio based on cell parameters
50:50	TFA:FFA solid solution	TFA:FFA crystals in 53:47 molar ratio.
60:40	TFA:FFA solid solution	TFA:FFA crystals in 60:40
80:20	TFA II and solid solution	FFA I, TFA II, and TFA:FFA solid solution

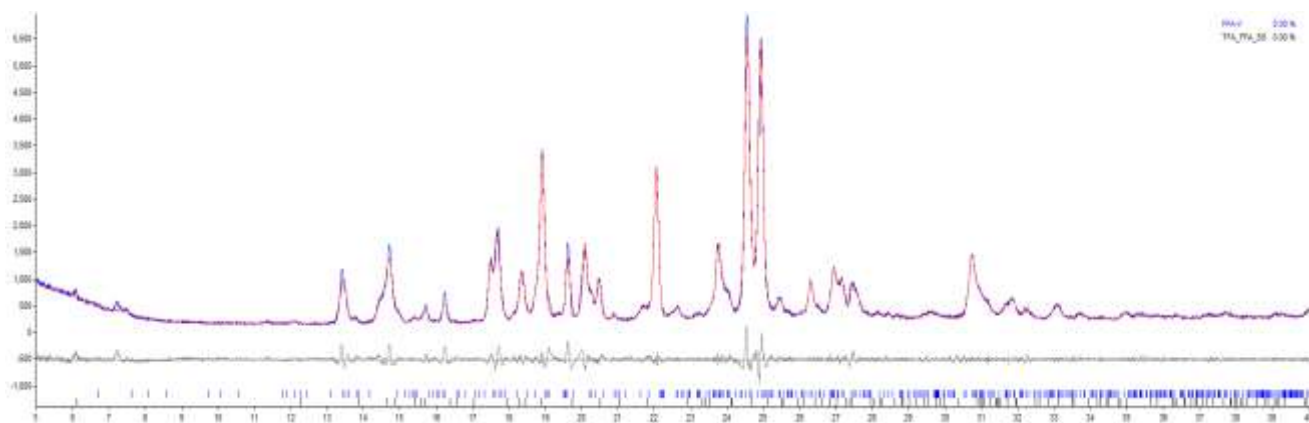


Figure S21. Pawley fit of the material obtained from crystallizing a 20:80 molar input of TFA:FFA material. The material is a mixture containing predominantly FFA V (blue markers) and TFA:FFA solid solution (black markers). The refined unit cell parameters of FFA V are: [$a=26.461(4)$ Å, $b=7.863(3)$ Å, $c=23.286(5)$ Å, $\alpha=90.0^\circ$, $\beta=94.65(9)^\circ$, $\gamma=90.0^\circ$] and TFA:FFA solid solution are: [$a=6.726(6)$ Å, $b=29.321(5)$ Å, $c=7.168(3)$ Å, $\alpha=90.0^\circ$, $\beta=112.89(6)^\circ$, $\gamma=90.0^\circ$]. The final residual values are $R_p=6.82\%$ and $R_{wp}=9.95\%$.

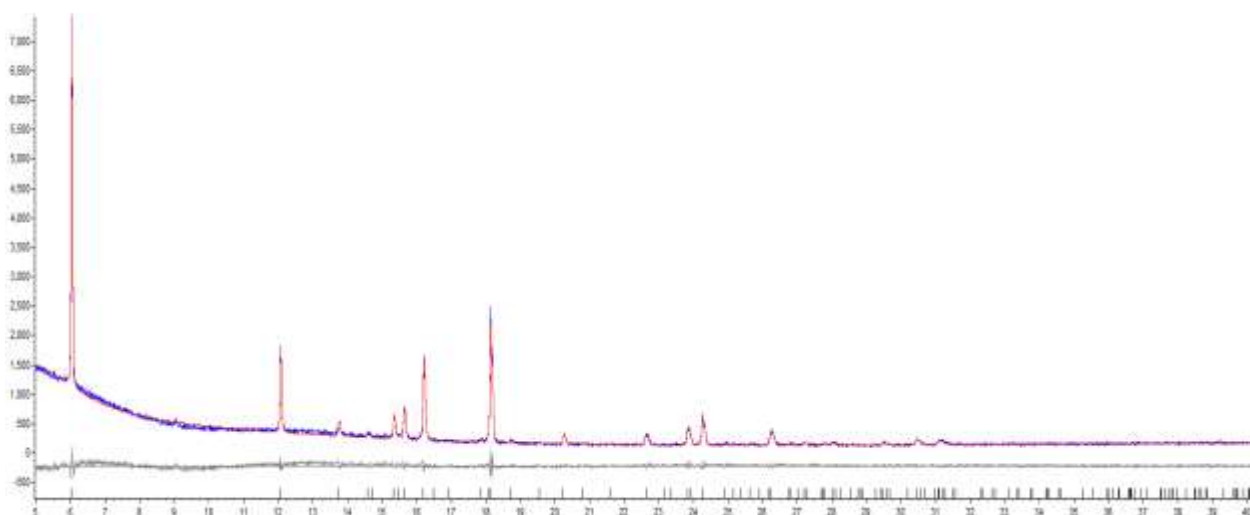


Figure S22. Pawley fit of TFA:FFA solid solution obtained from 50:50 molar input ratio using $(TFA)_{0.53}:(FFA)_{0.47}$ cell parameters. The refined cell parameters are: [$a=6.7329(4)$ Å, $b=29.331(4)$ Å, $c=7.153(5)$ Å, $\alpha=90.0^\circ$, $\beta=112.79(8)^\circ$, $\gamma=90.0^\circ$]. The final residual values of Pawley fit are $R_p=6.0\%$ and $R_{wp}=7.69\%$.

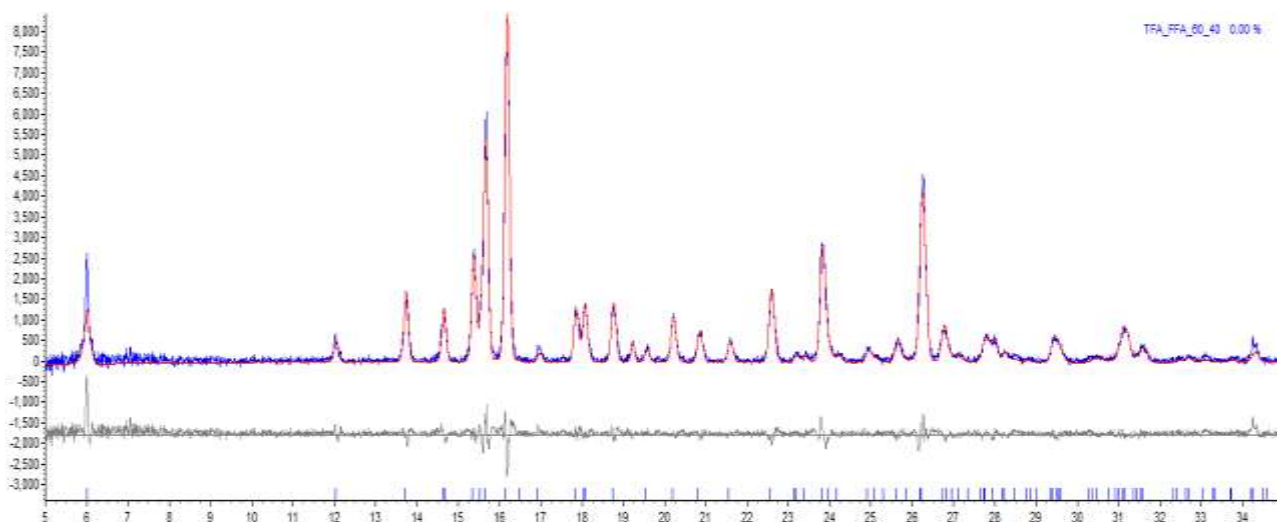


Figure S23. Pawley fit of TFA:FFA solid solution obtained from 60:40 molar input ratio using $(TFA)_{0.60}:(FFA)_{0.40}$ cell parameters. The refined cell parameters are: $[a=6.706(4) \text{ \AA}, b=29.421(1) \text{ \AA}, c=7.173(4) \text{ \AA}, \alpha=90.0^\circ, \beta=112.79(2)^\circ, \gamma=90.0^\circ]$. The final residual values of Pawley fit are $R_p=12.10\%$ and $R_{wp}=15.69\%$.

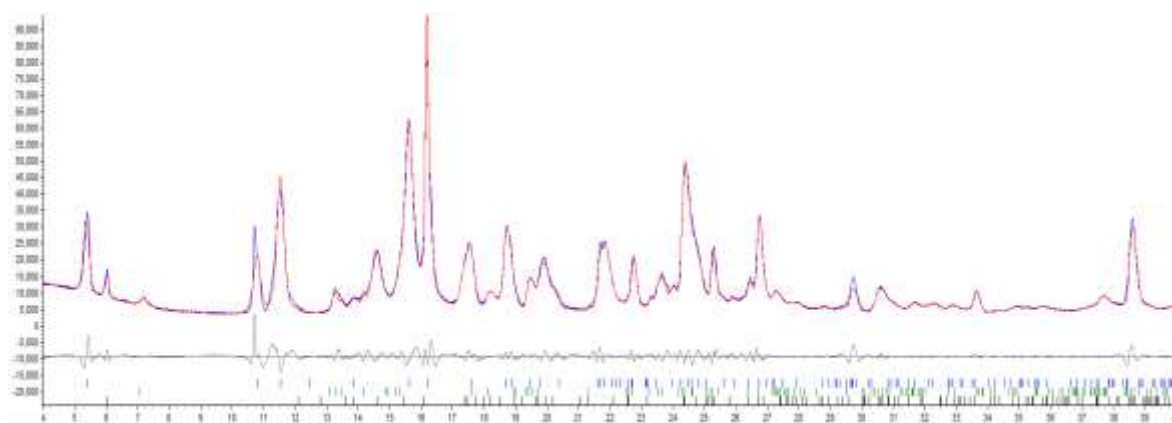


Figure S24. Pawley fit of the material obtained from 80:20 molar input ratio of TFA: FFA. The resulting material contains a mixture of TFA II (blue reflections) and TFA: FFA solid solution (black reflections) and FFA I (green reflections). The refined unit cell parameters of TFA II are: $[a=4.714(2) \text{ \AA}, b=32.459(3) \text{ \AA}, c=7.941(5) \text{ \AA}, \alpha=90.0^\circ, \beta=105.82(3)^\circ, \gamma=90.0^\circ]$, that of TFA:FFA solid solution are: $[a=6.729(3) \text{ \AA}, b=29.391(4) \text{ \AA}, c=7.143(5) \text{ \AA}, \alpha=90.0^\circ, \beta=113.11(6)^\circ, \gamma=90.0^\circ]$ and that of FFA I are: $[a=12.486(3) \text{ \AA}, b=7.886(1) \text{ \AA}, c=13.11253(7) \text{ \AA}, \alpha=90.0^\circ, \beta=94.91(4)^\circ, \gamma=90.0^\circ]$. The final residual values are $R_p=5.89\%$ and $R_{wp}=9.70\%$.

S7.1.9 Crystallization of TFA VII

Face indexing of $(TFA)_{0.53}:(FFA)_{0.47}$ solid solution crystals indicate that (010) is the dominant face in TFA:FFA crystals (Figure S25, Table S17).

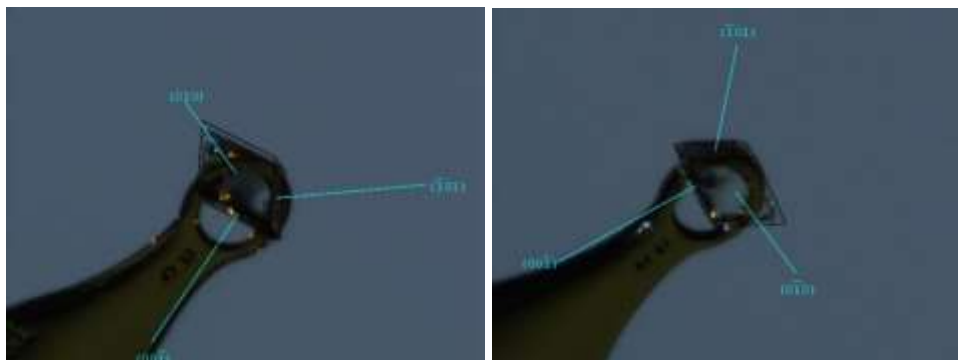


Figure S25. Face indexing $(TFA)_{0.53}:(FFA)_{0.47}$ crystals.

TFA VII crystals were obtained by vapour deposition of either TFA or TFA:FFA solid solution onto the (010) surface of TFA:FFA. Around 20 mg of either TFA or TFA:FFA solid solution was placed in a petri dish, which was placed on a heating plate held at 135 °C. The (010) surface of TFA:FFA single crystals mounted on a glass slide were exposed to TFA or TFA:FFA vapours for ~ 24 hrs. The resulting crystals were analyzed by single crystal X-ray diffraction (Table S17). TFA VII could be obtained by vapour deposition of either TFA or TFA:FFA solid solution material on the surface of TFA:FFA solids solution crystals.

S7.2 Single crystal X-ray diffraction

The single crystal X-ray diffraction data was collected using Cu-K α radiation ($\lambda=1.54184$ Å), on a Bruker D8-Venture diffractometer equipped with CMOS detector, controlled using APEX3 software. An Oxford Cryosystems Cryostream was used to cool the crystals to 150 K prior to data collection. Data integration and reduction were performed using the SAINT software. The crystal structures were solved by direct methods using the program SHELXS, and subsequent Fourier calculations and least-squares refinements were performed on F using the program CRYSTALS. All non-hydrogen atoms were refined with anisotropic displacement parameters. All hydrogen atoms bonded to the carbon atoms were placed geometrically and refined with the isotropic displacement parameter fixed at 1.5 times Ueq of the atoms to which they are attached. Protons involved in hydrogen bonding were located directly via inspection of difference Fourier maps and were refined isotropically.

Table S17. Crystallographic data of the solid solutions and polymorphs studied here.

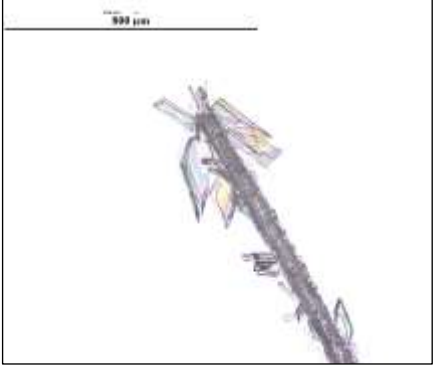
	TFA VI	(MFA) _{0.29} :(FFA) _{0.71}	(TFA) _{0.53} :(FFA) _{0.47}	(TFA) _{0.6} :(FFA) _{0.4}	TFA VII
chemical formula	C ₁₄ H ₁₂ Cl ₁ N ₁ O ₂	C ₁₄ H _{9.88} F _{2.12} N ₁ O ₂	C ₁₄ H _{10.58} Cl _{0.53} F _{1.42} N ₁ O ₂	C ₁₄ H _{10.82} Cl _{0.61} F _{1.18} N ₁ O ₂	C ₁₄ H ₁₂ Cl ₁ N ₁ O ₂
formula weight	261.7	264.36	270.4	268.9	261.7
crystal system	triclinic	Triclinic	monoclinic	monoclinic	monoclinic
a (Å)	6.7482(4)	6.7040(2)	6.6874(1)	6.7066(9)	6.7480(3)
b (Å)	7.2034(5)	7.226(2)	29.5208(6)	29.419(5)	29.153(4)
c (Å)	14.340(9)	15.404(4)	7.2115(1)	7.1728(13)	7.100(4)
α (°)	77.49(7)	78.29(3)	90	90	90
β (°)	78.94(7)	77.63(8)	112.79(1)	112.78(4)	112.82(3)
γ (°)	65.96(10)	66.67(1)	90	90	90
space group	P -1	P -1	P 2 ₁ /n	P 2 ₁ /n	P 2 ₁ /n
V/(Å) ³	617.3(4)	663.5(3)	1312.49(4)	1304.8(1)	1287.3(2)
Z/Z'	2/1	2/1	4/1	4/1	4/1

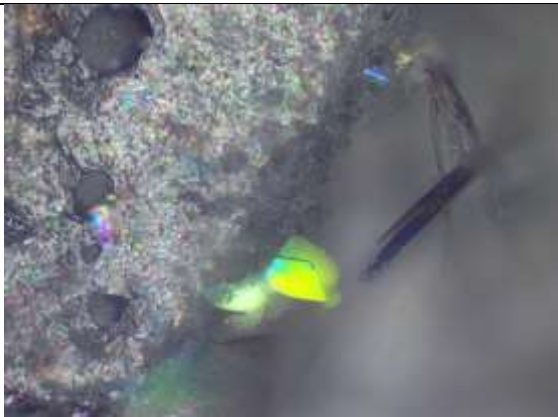
$N_{\text{reflection}}/$ $N_{\text{parameter}}$	1959/227	1351/198	1781/205	2103/205	1733/169
$\rho_{\text{calc}}/$ g/cm^3	1.408	1.323	1.369	1.369	1.347
radiation type	Cu K α ($\lambda=1.5418$ \AA)	Cu K α ($\lambda=1.5418$ \AA)	Cu K α ($\lambda=1.5418$ \AA)	Cu K α ($\lambda=1.5418$ \AA)	Cu K α ($\lambda=1.5418$ \AA)
T/K	150	293	293	293	293
range of h	-8 to 4	-9 to 9	-7 to 7	-7 to 7	-7 to 7
range of k	-8 to 8	-10 to 10	0 to 34	0 to 36	0 to 34
range of l	-17 to 16	-22 to 22	0 to 8	0 to 8	0 to 8
R_1 (%)	5.03	8.27	6.55	6.76	7.04
WR_2 (%)	15.38	18.04	6.08	6.81	8.40
goodness of fit	1.063	0.824	0.963	1.139	1.082

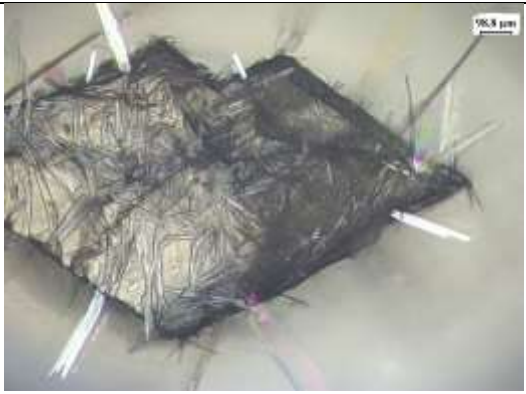
S7.2.1 Complete list of sublimation experiments

The material resulting from the sublimation experiments were analyzed by optical microscopy and by single crystal X-ray diffraction (SCXRD). In all the sublimation experiments we observe crystals growing laterally and vertically on the template surface, when analyzed by optical microscopy. While the lateral crystals are too small for SCXRD analysis, the vertical crystals were analyzed by SCXRD to confirm the polymorphic form of the sublimed material.

Table S18. Sublimation experiments attempted and the results. Green text highlights sublimation experiments that resulted in new polymorphs of TFA.

Sublimation material	Template polymorphic form	Result	Microscope images
MFA	TFA I	MFA I	

TFA	MFA I	TFA VI	
MFA	FFA III	MFA I and II	
TFA	FFA III	TFA I and II	
FFA	MFA I	FFA I and III	
FFA	TFA I	FFA I and III	crystals analyzed by SCXRD

TFA:FFA	TFA:FFA	TFA VII & II and FFA I	
FFA	TFA:FFA	FFA I and III	
MFA	TFA:FFA	MFA I	

S8. TFA Form VIII

S8.1 Preparation of TFA Form VIII

TFA VIII was prepared in a custom built high-vacuum chamber²⁵ connected to a heat source. The sample ca. 2g was placed in an aluminium oxide crucible heated by an OLED low temperature evaporator. Experiments were performed at temperatures in the range 100-150 °C and a deposition time of 3-4 hrs. Greatest phase purity was obtained on heating to 100 °C. The target for deposition was an ambient temperature copper disk (manually cleaned with Al₂O₃ 80 μm grit and ethanol) placed 250 mm from the evaporation source. This was equipped with a Quartz Crystal Microbalance (QCM) used to monitor deposition rates. On completion of the experiment the copper disk was removed and the sample carefully scrapped from the disk for subsequent PXRD analysis (Figure S26).

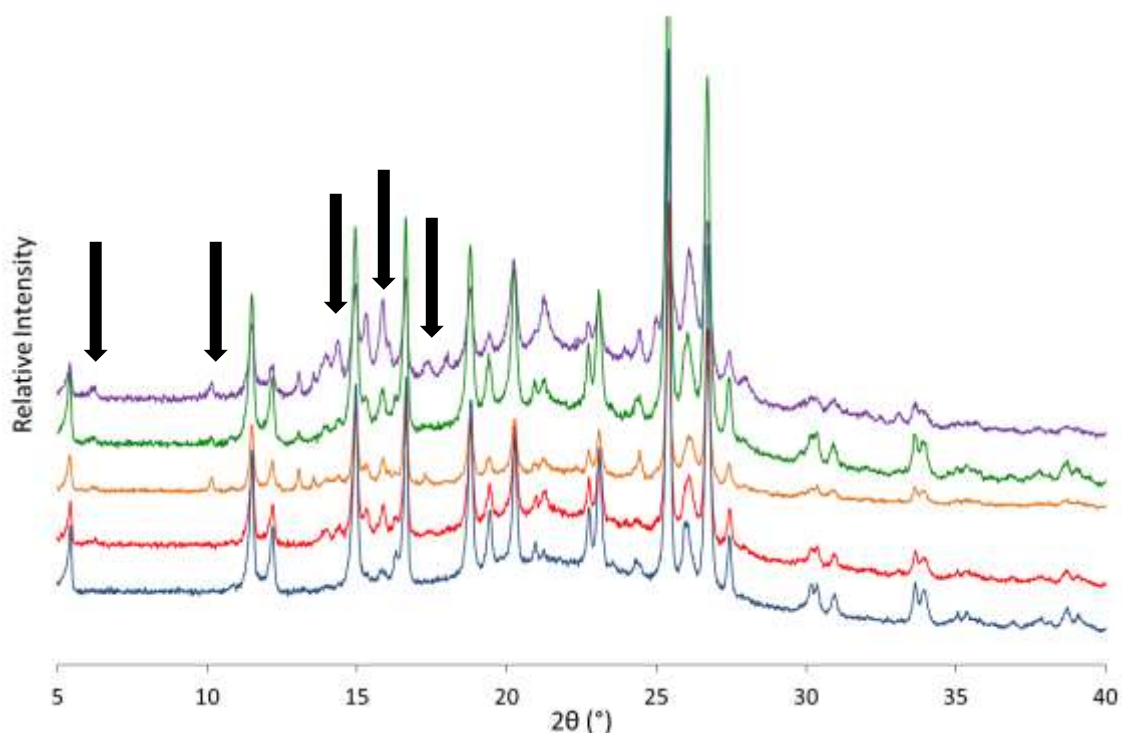


Figure S26. PXRD patterns of multiple depositions of TFA onto the copper surface. Top trace, fastest deposition rate (at 150 °C), bottom trace, slowest deposition rate (at 100 °C). The phase purity of TFA VIII increases from the top trace to the bottom trace. The additional peaks indicated by the black arrows are not attributed to TFA VIII. The bottom trace was indexed and used as the basis of the structure solution of TFA VIII from powder.

S8.2 Form VIII crystal structure

High-quality laboratory X-ray powder diffraction data were collected of the best sample of TFA form VIII mounted in a 0.5 mm capillary using a Stoe Stadi-P® diffractometer equipped with a Cu anode, Ge<111> monochromator providing a wavelength $\lambda=1.54056 \text{ \AA}$, a Dectris Mythen 1K® detector, and an Oxford Instruments CryojetHT® (90-500 K) with an in-house modified sample setup to minimize the formation of ice during sample rotation. A restricted beam-height collimator was used to minimize the effects of axial divergence. A PXRD pattern of the sample was measured at 120 K from 2° to 65° in 2 θ with a detector step size equal to 0.5° at 90 s per step and with a data step interval of 0.015°. The measurement was repeated four times giving a total acquisition time of about 16 hours and, after checking for reproducibility, the data were merged into a single scan file (C02522).

The PXRD pattern was indexed initially as triclinic ($a=16.718 \text{ \AA}$, $b=16.491 \text{ \AA}$, $c=8.005 \text{ \AA}$, $\alpha=94.74^\circ$, $\beta=80.92^\circ$, $\gamma=163.25^\circ$, $V=609.7 \text{ \AA}^3$) using the CRYSFIRE suite of programs.²⁶ Despite the use of a non-conventional unit cell, the crystal structure was solved in space group P-1 using the program FOX.²⁷ Starting with the known molecular geometry, the structure was solved using parallel tempering with relaxed restraints to provide a starting model for Rietveld refinement. The unit cell and structure were subsequently transformed to a triclinic cell with angles closer to 90° (Table S19). Rietveld refinement was performed using the Rietveld program PROFIL²⁸ (version 7.06). Given the limitations of laboratory PXRD, a single isotropic displacement parameter was used for all atoms and a chemically reasonable molecular geometry was maintained by the use of 81 bond distance and angle restraint functions based on the single-crystal study of TFA II at 110 K (CSD refcode KAXXAI). Non-H atoms for TFA in form VIII were labelled as for form II, but with the H atoms numbered according to the atom to which they are bonded as shown below:

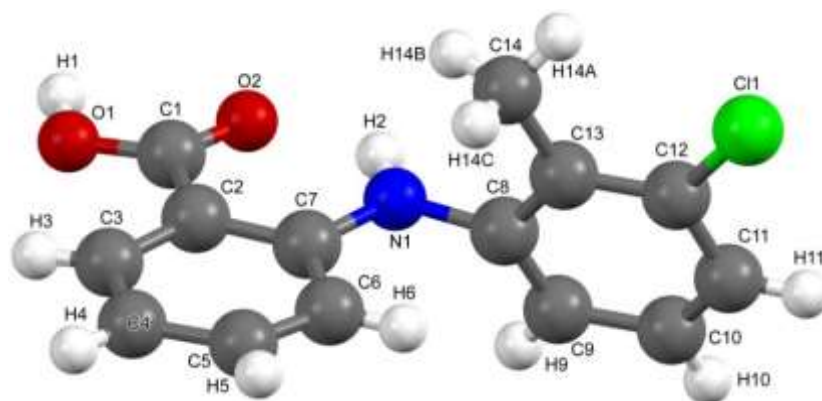


Figure S27. Atomic labelling of TFA VIII used in structural refinement (applicable to this section only).

Despite the use of soft restraint functions, the acid hydrogen atom H1 was not completely stable in the least-squares refinement. The best fit to the laboratory data is shown in Figure S28. Tables of the refined crystallographic parameters plus the PXRD data are available in the deposited CIF file. In TFA VIII, the dihedral angle defined by the planes of the benzoic acid ring and the chlorophenyl ring is 75° (compared to 43° in form II).

Table S19. Comparison of the unit cells of the triclinic form VIII and the monoclinic form II of TFA.

Form	$a / \text{Å}$	$b / \text{Å}$	$c / \text{Å}$	$\alpha / ^\circ$	$\beta / ^\circ$	$\gamma / ^\circ$	$V / Z / \text{Å}^3$
VIII	8.0025(5)	16.4742(11)	4.8422(3)	95.735(4)	105.222(5)	94.752(4)	304.47(4)
II	3.836(2)	21.997(5)	14.205(7)	90	94.11(4)	90	298.89

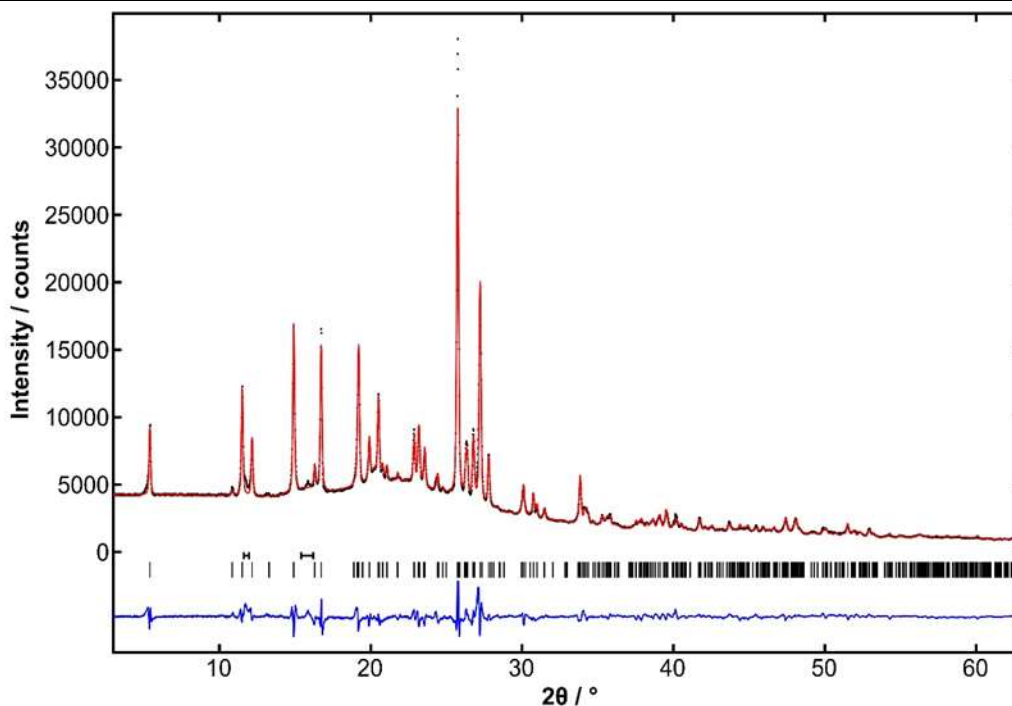


Figure S28. Rietveld refinement plot showing the fit of the structure of form VIII to the laboratory PXRD data. Measured data points are shown as black dots, the calculated PXRD pattern as a red line, calculated reflection positions with vertical tick bars, and the difference between observed and calculated patterns in blue. Due to a trace of polymorph impurity, two small regions of the pattern, shown by horizontal bars in the plot above, were zero weighted in the least-squares refinement.

S8.3 Sublimation Studies using QBox

Crystalline films containing TFA VIII were prepared on smooth substrates by controlled sublimation experiments²⁹ performed using a custom-made QBox 450 deposition system (Mantis Deposition Ltd., Thame, U.K.). An alumina coated crucible was used for subliming the starting material (TFA powder, 99+%, Alfa Aesar) and a QCM sensor was positioned close to the crucible to enable the rate of vapor deposition and thickness of the sublimed TFA onto experimental substrates to be monitored in real time. The nanoscale roughness of all substrates employed was assessed using a Bruker Dimension FastScan AFM instrument prior to experiments commencing. The substrates were cut into either 1 cm x 1 cm or 2 cm x 2 cm tiles and placed face down in a multi-position sample holder positioned 14 cm above the crucible. During the vapor deposition process, the holder was constantly rotated at 20 rpm to ensure equal distribution of the deposited material. The TITANIUM software by Mantis Deposition Ltd was utilized to monitor the deposition rate and sample thickness for each experiment. Before any experiments were performed, the QBox was vented to atmospheric pressure and then pumped down to a high vacuum (pressure $\leq 9.99 \times 10^{-7}$ Torr). In order for sublimation of TFA to commence, an electric current of 0.35 V was applied to the crucible in the first instance and the TITANIUM software was used to manipulate the voltage in small increments until the rate of deposition began to increase. The temperature of the powder in the crucible was monitored at all times by using a thermocouple. At the end of each experiment, a shutter positioned between the crucible and the sample holder was closed to prevent further TFA depositing on the substrates.

All TFA samples prepared using the QBox system were characterized using PXRD in reflection geometry (see Section S7 for details of the D8 Discover diffractometer). The samples were placed on silicon low background holders and measurements were obtained under ambient conditions in the scan range of 3-35° 2 θ using a step size of 0.01° and count time of 30 s/step. Raman spectroscopy was additionally performed using an XploRA PLUS Raman microscope by HORIBA Scientific which was equipped with a motorized x-y-z stage, 50x objective lens and 785 nm excitation laser. The spectra collected were compared with reference Raman data for TFA polymorphs (Figure S30).⁵

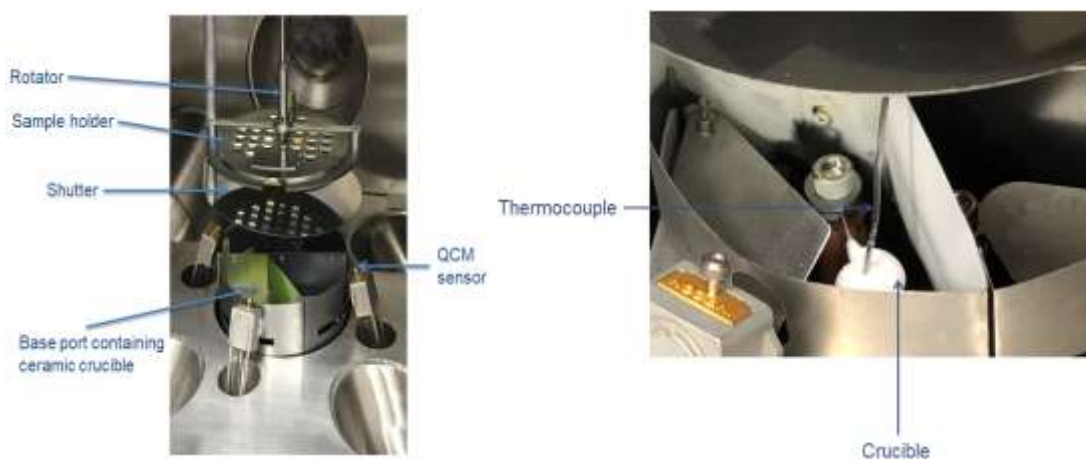


Figure S29. Experimental setup for sublimation experiments with the QBox 450 deposition system.

Controlled sublimation of TFA onto rough copper foil substrates using slow, medium and fast deposition rates (Table S20) resulted in the formation of films corresponding to a mixture of polymorphs I & IV (Figure S30). When smooth copper-coated and silver-coated glass coverslips were used as substrates (Table S21), slow deposition rates resulted in mixture of polymorphs I, IV and VIII (Figure S31-Figure S32). Due to the poor signal to noise ratio of the powder data reliable

Pawley profile fitting of the powder patterns in Figure S31 and Figure S32 has not been possible. Whilst these patterns show peak positions that coincide with TFA I and TFA IV at low angles, the peaks at $\sim 12.17, 14.95^\circ 2\theta$ are coincident with TFA VIII and are not observed in either TFA I or TFA IV, providing a basis to conclude that the sample comprises of a small amount of TFA VIII in addition to TFA I and IV.

Table S20. Overview of experimental conditions for the deposition of TFA onto copper foil substrates with R_a roughness of 99 nm. The copper substrates were cleaned using isopropanol and deionized water and dried under a stream of argon prior to experimental use.

Average deposition rate ($\text{\AA}/\text{s}$)	QCM estimate for film thickness (μm)	Average sublimation temperature ($^\circ\text{C}$)	Polymorphic form
1.9 (slow)	1.7	97	I & IV
3.9 (medium)	1.7	100	I & IV
5.9 (fast)	1.7	111	I & IV

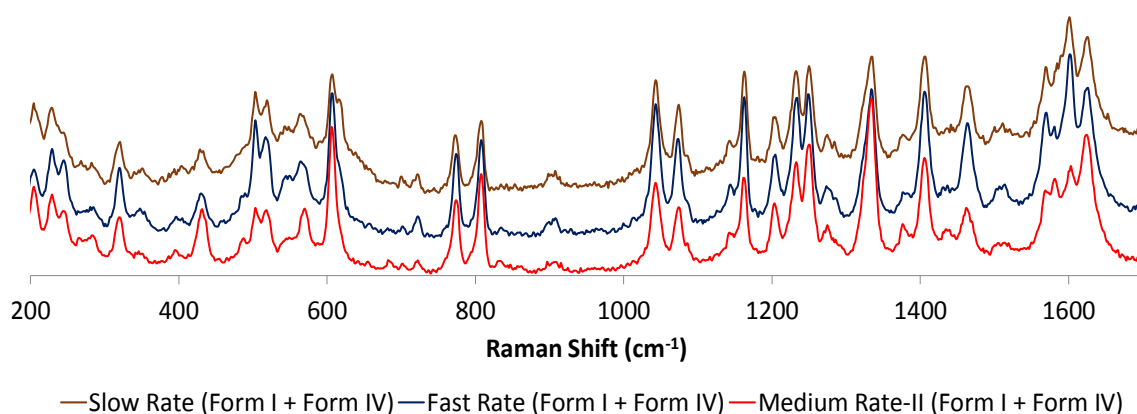


Figure S30. Overlay of Raman spectra of TFA films grown on copper foil substrates using different deposition rates.

Table S21. Overview of experimental conditions for the slow deposition of TFA onto copper-coated (R_a roughness = 1 nm) and silver-coated (R_a roughness = 2.4 nm) glass substrates. The substrates were fabricated by controlled deposition of ~ 200 nm of copper and silver onto glass coverslips and were used without applying further cleaning procedures.

Average deposition rate ($\text{\AA}/\text{s}$)	QCM estimate for film thickness	Average sublimation temperature ($^\circ\text{C}$)	Polymorphic form
2	1 μm	117	I + IV + VIII
1.5	500 nm	109	I + IV + VIII

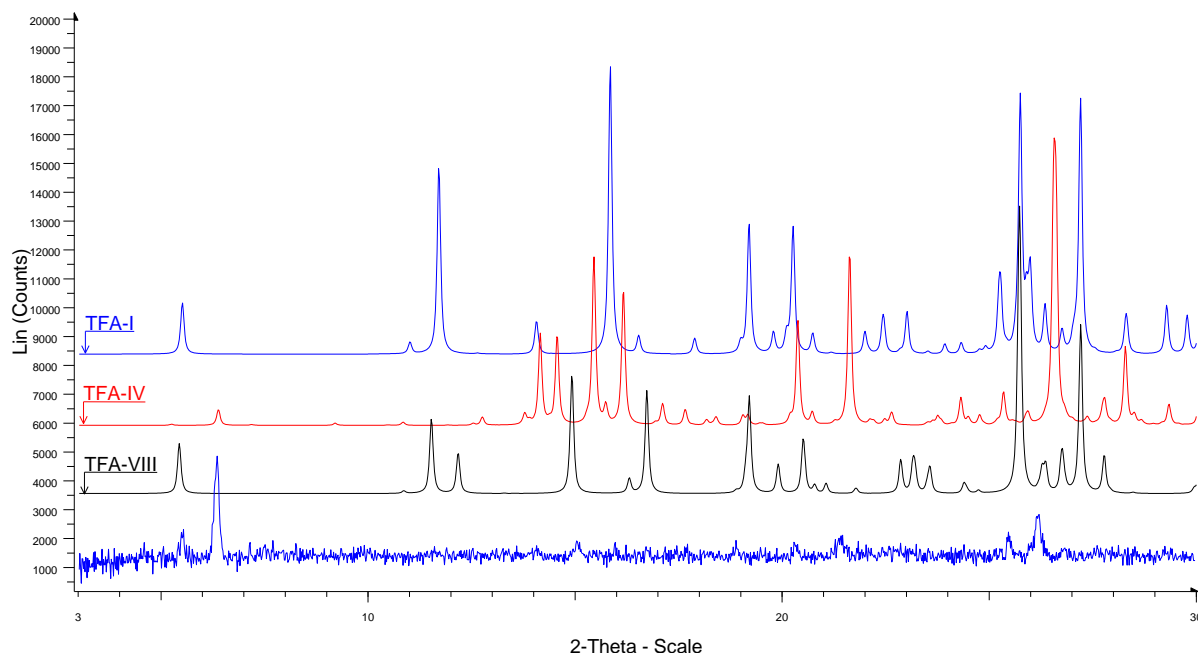


Figure S31. Reflection geometry PXRD analysis of TFA films prepared via sublimation onto copper-coated glass. The peak at $14.95^\circ 2\theta$ is representative of TFA VIII and not observed in TFA I and TFA IV.

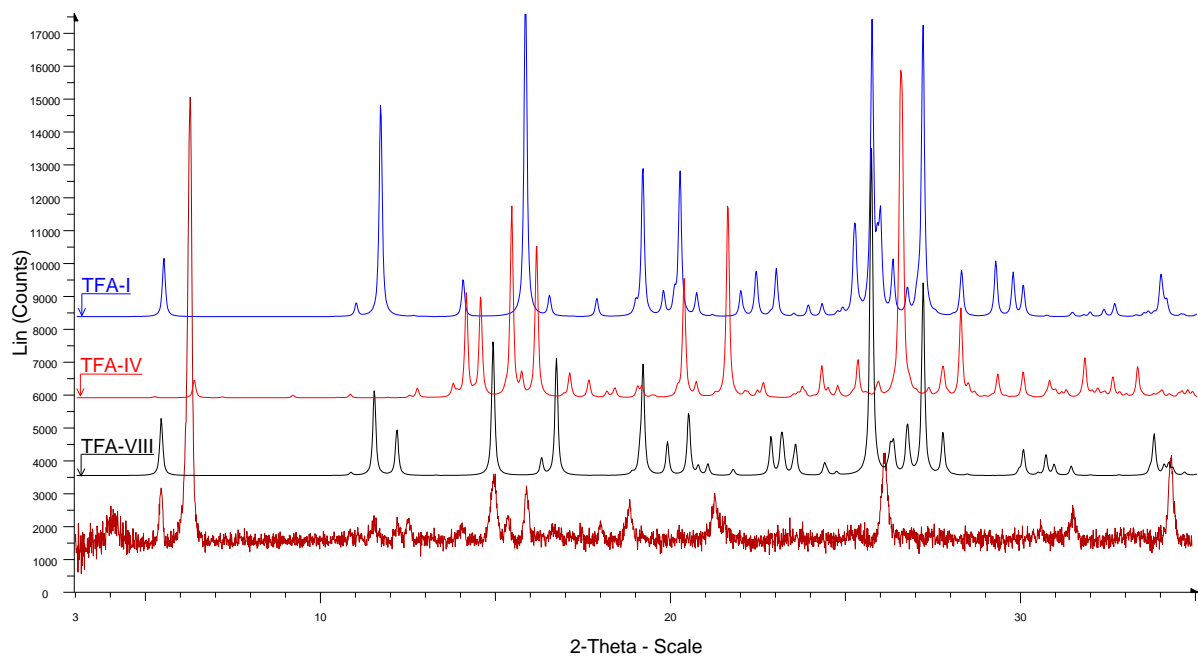


Figure S32. Reflection geometry PXRD analysis of TFA films prepared via sublimation onto silver-coated glass. The broad feature at ca. $4^\circ 2\theta$ is attributed to scattering from the substrate and the peaks at $\sim 12.17^\circ$ and $14.95^\circ 2\theta$ are representative peaks of TFA VIII and are not observed in TFA I and TFA IV.

S9. Reproduction of experimental and isostructural crystal cell parameters by various computational models.

Table S22. Cell parameters for MFA, in the structures listed in the leftmost column. The second column details whether the data is experimental or from a CrystalOptimizer (CO), PCM, or PBE-TS calculation. Experimental parameters for structures not containing the MFA molecule are those of the TFA, FFA, or solid solution structure, accounting for the deviation from the computationally minimized structures.

Structure	From	MFA					
		a/Å	b/Å	c/Å	$\alpha/^\circ$	$\beta/^\circ$	$\gamma/^\circ$
MFA I	expt	14.56	6.81	7.66	119.57	103.93	91.30
	CO	14.23	6.98	7.67	119.05	102.82	93.96
	PCM	14.21	6.96	7.66	118.87	103.04	93.86
	PBE-TS	14.16	6.71	7.60	119.21	104.88	91.24
MFA II maj	expt	7.70	9.12	9.45	107.11	91.79	101.48
	CO	7.97	8.75	9.86	109.72	95.70	97.79
	PCM	7.98	8.73	9.83	109.53	95.67	97.73
	PBE-TS	7.65	8.81	9.57	108.02	92.74	100.07
MFA II min	expt	7.70	9.12	9.45	107.11	91.79	101.48
	CO	8.56	7.92	10.54	114.39	102.25	92.43
	PCM	8.56	7.92	10.50	114.13	102.14	92.49
	PBE-TS	8.72	7.30	10.75	115.95	104.76	89.88
MFA III	expt	7.72	7.93	11.23	83.59	80.94	67.51
	CO	7.80	8.30	11.13	76.90	81.09	62.39
	PCM	7.81	8.29	11.12	77.14	81.08	62.33
	PBE-TS	7.65	8.28	11.48	74.91	81.09	56.46
TFA I	expt	4.83	32.13	8.04	90.00	104.88	90.00
	CO	5.01	31.16	8.79	90.00	67.31	90.00
	PCM	5.01	31.12	8.79	90.00	67.22	90.00
	PBE-TS	4.72	31.72	8.42	90.00	69.83	90.00
TFA II	expt	3.84	22.00	14.21	90.00	94.11	90.00
	CO	4.00	22.44	14.44	90.00	93.97	90.00
	PCM	4.01	22.43	15.26	90.00	70.23	90.00
	PBE-TS	3.79	22.13	14.88	90.00	71.24	90.00
TFA III	expt	7.64	11.31	28.07	90.00	93.03	90.00
	CO	7.87	11.80	27.40	90.00	85.99	90.00
	PCM	7.85	11.81	27.39	90.00	85.79	90.00
	PBE-TS	6.92	6.92	26.98	87.24	87.24	111.33
TFA IV	expt	7.52	14.33	17.59	103.68	98.25	93.04
	CO	6.96	7.43	14.01	103.24	99.40	64.21
TFA Va	expt	7.65	9.02	9.42	107.39	92.06	101.66
	CO	8.14	8.52	9.94	69.78	96.27	82.83
	PCM	8.14	8.52	9.91	70.08	96.15	82.73
	PBE-TS	8.00	8.29	9.85	70.30	95.55	83.17
TFA Vb	expt	7.65	9.02	9.42	107.39	92.06	101.66
	CO	9.85	7.94	8.77	97.94	70.47	84.44

TFA VIa	expt	6.80	7.40	14.10	77.00	80.30	65.60
	CO	6.96	7.43	14.01	103.24	99.40	64.21
	PCM	6.96	7.44	13.98	103.24	99.55	64.11
	PBE-TS	6.72	7.29	13.93	103.34	101.17	65.64
TFA VIb	expt	6.80	7.10	14.50	78.80	81.30	65.80
	CO	6.96	7.43	14.01	103.24	99.40	64.21
	PCM	6.96	7.44	13.98	103.24	99.55	64.11
	PBE-TS	6.72	7.29	13.93	103.34	101.17	65.64
TFA VII	expt	6.75	29.15	7.10	90.00	112.83	90.00
	CO	7.07	28.23	7.01	90.00	66.86	90.00
	PCM	7.07	28.21	7.01	90.00	66.79	90.00
	PBE-TS	6.83	27.72	6.92	90.00	68.24	90.00
TFA VIII	expt	4.80	8.50	15.80	100.40	91.10	100.60
	CO	5.12	8.39	14.88	80.11	93.81	81.94
	PCM	5.12	8.39	14.86	80.23	93.91	82.00
	PBE-TS	4.88	8.28	15.14	81.01	94.38	81.54
FFA I	expt	12.52	7.87	12.87	90.00	95.20	90.00
	CO	10.88	8.10	14.78	90.00	100.50	90.00
	PCM	16.67	8.09	14.76	90.00	39.96	90.00
	PBE-TS	16.36	7.91	14.70	90.00	38.19	90.00
FFA II	expt	10.88	10.24	11.75	90.00	111.32	90.00
	CO	11.15	10.29	11.79	90.00	110.31	90.00
	PCM	11.16	10.27	11.82	90.00	110.47	90.00
	PBE-TS	10.97	9.96	11.77	90.00	111.62	90.00
FFA III	expt	39.85	5.11	12.24	90.00	92.47	90.00
	CO	36.68	7.83	9.86	90.00	111.67	90.00
	PCM	36.64	7.82	9.87	90.00	111.69	90.00
	PBE-TS	36.76	7.71	9.17	90.00	109.46	90.00
MFA:TFA	expt	6.75	7.32	14.18	77.09	79.77	65.32
	CO	6.95	7.36	14.14	77.54	80.30	64.70
	PCM	6.94	7.36	14.12	77.58	80.13	64.63
	PBE-TS	6.72	7.29	13.93	103.34	101.17	65.64
MFA:FFA	expt	6.70	7.22	15.40	91.48	102.19	113.18
	CO	6.94	7.37	14.69	90.47	108.22	115.32
	PCM	6.93	7.37	14.65	90.40	108.08	115.38
	PBE-TS	6.72	7.29	13.93	103.34	101.17	65.64
TFA:FFA	expt	6.69	29.52	7.21	90.00	112.79	90.00
	CO	7.07	28.23	7.01	90.00	66.86	90.00
	PCM	7.07	28.21	7.01	90.00	66.79	90.00
	PBE-TS	6.83	27.72	6.92	90.00	68.24	90.00

Table S23. Cell parameters for TFA, in the structures listed in the leftmost column. The second column details whether the data is experimental or from a CrystalOptimizer (CO), with a polarizable continuum model (PCM), periodic density functional theory with dispersion (PBE-TS) or experiment. Experimental parameters for structures not containing the TFA molecule are those of the MFA, FFA, or solid solution structure, accounting for the deviation from the computationally minimized structures. For TFA VII, the calculated values for the isomorphous TFA:FFA structure can be used.

Structure	From	TFA					
		a/Å	b/Å	c/Å	$\alpha/^\circ$	$\beta/^\circ$	$\gamma/^\circ$
MFA I	expt	14.56	6.81	7.66	119.57	103.93	91.3
	CO	7.11	7.05	13.96	102.57	80.94	112.96
	PCM	7.1	7.05	13.98	102.82	80.97	112.89
	PBE-TS	14.77	6.88	7.76	124.34	110.72	85.86
MFA II maj	expt	7.7	9.12	9.45	107.11	91.79	101.48
	CO	9.5	10.77	7.64	122.13	92.88	72.92
	PCM	9.52	10.77	7.66	122.58	93.17	72.87
	PBE-TS	7.55	9.16	9.38	106.16	90.32	102.85
MFA II min	expt	7.7	9.12	9.45	107.11	91.79	101.48
	CO	8.65	7.59	11.02	117.04	105.39	91.31
	PCM	8.66	7.56	11	116.87	105.34	91.36
	PBE-TS	8.75	7.21	11.09	117.4	105.96	89.26
MFA III	expt	7.72	7.93	11.23	83.59	80.94	67.51
	CO	7.78	7.9	11.47	79.81	98.31	64.78
	PCM	7.74	7.89	11.45	79.88	98.35	65.03
	PBE-TS	7.65	8.24	11.56	74.28	80.96	56.75
TFA I	expt	4.83	32.13	8.04	90	104.88	90
	CO	4.86	31.7	8.31	90	102.37	90
	PCM	4.86	31.65	8.31	90	102.28	90
	PBE-TS	4.69	32.25	8.08	90	103.96	90
TFA II	expt	3.84	22	14.21	90	94.11	90
	CO	3.86	22.1	14.62	90	95.96	90
	PCM	3.86	22.07	14.59	90	96.29	90
	PBE-TS	3.75	21.85	14.43	90	95.29	90
TFA III	expt	7.64	11.31	28.07	90	93.03	90
	CO	7.81	11.6	27.67	90	93.03	90
	PCM	7.8	11.61	27.65	90	93.22	90
	PBE-TS	7.79	11.27	27.46	90	94.84	90
TFA IV	expt	7.52	14.33	17.59	103.68	98.25	93.04
	CO	7.65	14.01	18.34	102.48	99.33	91.59
	PCM	7.65	14.02	18.27	102.52	99.31	91.47
	PBE-TS	7.77	14.11	17.49	104.89	102.83	84.55
TFA Va	expt	7.65	9.02	9.42	107.39	92.06	101.66
	CO	7.63	9.31	9.52	107.41	93.04	101.67
	PCM	7.65	9.25	9.54	107.32	93.33	101.44
	PBE-TS	8.75	7.21	11.09	117.4	105.96	89.26
TFA Vb	expt	7.65	9.02	9.42	107.39	92.06	101.66
	CO	6.8	10.67	9.03	93.78	85.27	103.28

	PCM	6.79	10.71	9.02	93.2	85.29	103.37
	PBE-TS	7.55	9.16	9.37	106.13	90.26	102.91
TFA VIa	expt	6.8	7.4	14.1	77	80.3	65.6
	CO	7.04	7.12	13.98	80.88	77.49	67.07
	PCM	7.03	7.1	13.99	80.91	77.25	67.15
	PBE-TS	6.90	6.93	14.02	81.56	75.31	68.36
TFA VIb	expt	6.8	7.1	14.5	78.8	81.3	65.8
	CO	6.96	7.31	14.09	78.04	80.29	64.64
	PCM	6.94	7.3	14.09	78.09	80.21	64.75
	PBE-TS	6.88	6.88	14.12	81.6	75.32	68.63
TFA VII	expt	6.75	29.15	7.1	90	112.83	90
	CO	6.53	30.61	6.86	90	111.18	90
	PCM	6.54	30.52	6.85	90	111.19	90
	PBE-TS	6.38	29.84	6.94	90.00	111.21	90.00
TFA VIII	expt	4.8	8.5	15.8	100.4	91.1	100.6
	CO	4.83	8.47	15.79	100.37	91.1	100.72
	PCM	4.83	8.46	15.79	100.23	91.21	100.64
	PBE-TS	4.7	8.1	16.45	96.93	93.94	103.94
FFA I	expt	12.52	7.87	12.87	90	95.2	90
	CO	15.9	7.74	10.21	90	86.12	90
	PCM	15.89	7.73	10.18	90	86.18	90
	PBE-TS	15.98	7.65	9.9	90	86.44	90
FFA II	expt	10.88	10.24	11.75	90	111.32	90
	CO	11.07	10.32	12.07	90	113.32	90
	PCM	11.05	10.32	12.08	90	113.56	90
	PBE-TS	10.82	10.06	11.90	90	112.76	90
FFA III	expt	39.85	5.11	12.24	90	92.47	90
	CO	36.67	7.89	9.55	90	110.39	90
	PCM	36.58	7.89	9.59	90	110.47	90
	PBE-TS	37.1	7.76	8.92	90	107.93	90
MFA:TFA	expt	6.75	7.32	14.18	77.09	79.77	65.32
	CO	6.93	7.3	14.12	78.07	80.15	64.76
	PCM	6.91	7.29	14.11	78.11	80.08	64.86
	PBE-TS	14.77	6.88	7.76	124.34	110.72	85.86
MFA:FFA	expt	6.70	7.23	15.40	91.48	102.19	113.18
	CO	7.11	7.05	13.96	102.57	80.94	112.96
	PCM	7.1	7.05	13.98	102.82	80.97	112.89
	PBE-TS	14.77	6.88	7.76	124.34	110.72	85.86
TFA:FFA	expt	6.69	29.52	7.21	90	112.79	90
	CO	6.53	30.61	6.86	90	111.18	90
	PCM	6.54	30.52	6.85	90	111.19	90
	PBE-TS	6.38	29.84	6.94	90	111.21	90

Table S24. Cell parameters for FFA, in the structures listed in the leftmost column. The second column details whether the data is experimental or from a CrystalOptimizer (CO), PCM, or PBE-TS calculation. Experimental parameters for structures not containing the FFA molecule are those of the MFA, TFA, or solid solution structure, accounting for the deviation from the computationally minimized structures.

Structure	From	FFA					
		a/Å	b/Å	c/Å	$\alpha/^\circ$	$\beta/^\circ$	$\gamma/^\circ$
MFA I	expt	14.56	6.81	7.66	119.57	103.93	91.30
	CO	15.03	7.31	6.56	68.30	102.14	88.01
	PCM	14.97	7.31	6.58	68.28	102.12	88.05
	PBE-TS	15.81	7.26	5.98	68.40	96.77	84.04
MFA II maj	expt	7.70	9.12	9.45	107.11	91.79	101.48
	CO	7.77	9.71	8.89	102.89	86.57	104.72
	PCM	7.77	9.69	8.89	102.64	86.55	104.48
MFA II min	expt	7.70	9.12	9.45	107.11	91.79	101.48
	CO	10.63	7.16	11.47	127.95	111.74	81.59
	PCM	10.64	7.11	11.44	127.44	111.70	81.96
MFA III	expt	7.72	7.93	11.23	83.59	80.94	67.51
	CO	8.33	10.27	10.31	64.69	81.25	57.48
	PCM	8.40	10.23	10.29	64.66	80.91	57.41
	PBE-TS	7.32	10.20	11.16	67.07	83.33	57.56
TFA I	expt	4.83	32.13	8.04	90.00	104.88	90.00
	CO	4.76	29.46	9.04	90.00	96.03	90.00
	PCM	4.77	29.39	9.04	90.00	96.40	90.00
	PBE-TS	4.65	29.84	8.95	90.00	97.33	90.00
TFA II	expt	3.84	22.00	14.21	90.00	94.11	90.00
	CO	4.18	22.22	14.43	90.00	95.09	90.00
	PCM	4.19	22.20	14.41	90.00	95.34	90.00
	PBE-TS	4.52	18.22	15.49	90.00	104.35	90.00
TFA III	expt	7.64	11.31	28.07	90.00	93.03	90.00
	CO	7.88	11.56	28.69	90.00	85.83	90.00
	PCM	7.88	11.55	28.67	90.00	85.75	90.00
	PBE-TS	7.69	11.13	29.70	90.00	85.50	90.00
TFA Va	expt	7.65	9.02	9.42	107.39	92.06	101.66
	CO	7.77	9.69	8.91	102.99	86.69	104.60
	PCM	7.77	9.68	8.90	102.70	86.65	104.43
TFA VIa	expt	6.80	7.40	14.10	77.00	80.30	65.60
	CO	15.03	7.31	6.56	68.30	102.14	88.01
	PCM	14.97	7.31	6.58	68.28	102.12	88.05
	PBE-TS	15.81	7.26	5.98	68.40	96.77	84.04
TFA VIb	expt	6.80	7.10	14.50	78.80	81.30	65.80
	CO	15.03	7.31	6.56	68.30	102.14	88.01
	PCM	14.97	7.31	6.58	68.28	102.12	88.05
	PBE-TS	15.81	7.26	5.98	68.40	96.77	84.04
TFA VII	expt	6.75	29.15	7.10	90.00	112.83	90.00
	CO	6.53	28.96	7.90	90.00	60.47	90.00

	PCM	6.52	28.98	7.88	90.00	60.39	90.00
	PBE-TS	6.13	30.24	7.68	90.00	61.61	90.00
TFA VIII	expt	4.80	8.50	15.80	100.40	91.10	100.60
	CO	4.76	16.37	9.06	71.31	86.33	107.03
	PCM	4.68	15.74	8.77	96.26	100.69	77.74
	PBE-TS	4.62	15.74	8.64	98.72	101.96	78.53
FFA I	expt	12.52	7.87	12.87	90.00	95.20	90.00
	CO	12.06	7.97	12.91	90.00	94.99	90.00
	PCM	12.10	7.97	12.85	90.00	95.05	90.00
	PBE-TS	12.00	7.89	12.72	90.00	95.83	90.00
FFA II	expt	10.88	10.24	11.75	90.00	111.32	90.00
	CO	10.81	10.41	11.66	90.00	110.33	90.00
	PCM	10.80	10.41	11.69	90.00	110.63	90.00
	PBE-TS	10.49	10.37	11.91	90.00	112.58	90.00
FFA III	expt	39.85	5.11	12.24	90.00	92.47	90.00
	CO	39.98	5.12	12.16	90.00	91.08	90.00
	PCM	39.90	5.11	12.19	90.00	91.00	90.00
	PBE-TS	39.90	4.90	12.09	90.00	91.78	90.00
FFA IV	expt	8.76	11.66	20.02	80.63	81.04	73.53
	CO	8.71	11.43	20.03	80.81	81.15	77.83
	PCM	8.73	11.43	20.01	80.62	80.98	77.77
	PBE-TS	9.05	10.88	20.33	78.49	79.90	69.99
FFA V	expt	26.66	7.90	23.24	90.00	94.08	90.00
	CO	27.30	8.28	22.64	90.00	93.51	90.00
	PCM	27.33	8.26	22.65	90.00	93.24	90.00
FFA VI	expt	8.65	11.51	38.90	87.91	85.91	72.26
	CO	9.03	11.34	39.63	85.68	85.49	72.89
	PCM	9.05	11.38	39.48	85.76	85.41	72.72
FFA VII	expt	14.97	20.64	7.95	90.00	98.32	90.00
	CO	15.09	21.02	7.91	90.00	97.20	90.00
	PCM	15.07	20.99	7.92	90.00	97.50	90.00
	PBE-TS	14.48	21.19	7.89	90.00	97.71	90.00
MFA:TFA	expt	6.75	7.32	14.18	77.09	79.77	65.32
	CO	6.53	28.96	7.90	90.00	60.47	90.00
	PCM	14.97	7.31	6.58	68.28	102.12	88.05
	PBE-TS	15.81	7.26	5.98	68.40	96.77	84.04
MFA:FFA	expt	6.70	7.23	15.40	91.48	102.19	113.18
	CO	6.54	7.31	15.06	92.07	102.11	111.66
	PCM	6.56	7.31	15.00	92.03	102.09	111.68
	PBE-TS	15.81	7.26	5.98	68.40	96.77	84.04
TFA:FFA	expt	6.69	29.52	7.21	90.00	112.79	90.00
	CO	6.52	28.94	7.37	90.00	110.95	90.00
	PCM	6.52	28.95	7.35	90.00	110.97	90.00
	PBE-TS	6.13	30.24	7.68	90.00	61.61	90.00

S10. CSP Structures

The computer generated structures are available from the UCL authors on request in .res format. Table S25-Table S27 give the structure label (which uses the rank after CrystalPredictor), space group, unit cell parameters, and lattice energy for the lowest 100 computationally generated structures in the CEL at the PCM level of theory for each molecule.

Table S25. CEL for MFA at the PCM level of theory.

Label	Space Group	a /Å	b /Å	c /Å	α /°	β /°	γ /°	Lattice Energy /kJ/mol
M128	P -1	6.96	7.44	13.98	103.24	99.55	64.11	-147.72
M237	P 1 21/c 1	13.30	7.02	15.85	90.00	59.41	90.00	-146.48
M889	P -1	9.83	7.95	8.75	97.88	70.66	84.47	-145.97
M510	P -1	5.12	8.39	14.86	80.23	93.91	82.00	-145.87
M288	C 1 2/c 1	7.85	11.81	27.39	90.00	85.79	90.00	-145.06
M1666	P -1	8.30	11.12	7.81	81.07	117.81	103.03	-144.79
M2853	P 1 21 1	7.07	28.21	7.01	90.00	66.79	90.00	-144.66
M1592	P 1 21 1	7.00	28.18	7.07	90.00	66.82	90.00	-144.63
M5611	P 1 21 1	7.75	28.17	7.01	90.00	56.98	90.00	-144.60
M1069	P b c a	23.15	15.63	7.07	90.00	90.00	90.00	-144.22
M1090	P b c a	23.16	15.57	7.10	90.00	90.00	90.00	-144.08
M664	P b c a	22.95	16.14	7.00	90.00	90.00	90.00	-143.38
M318	C 1 2/c 1	24.59	6.88	16.31	90.00	67.58	90.00	-143.27
M538	P 1 21/c 1	11.90	6.90	16.29	90.00	72.74	90.00	-143.12
M1055	A 1 2/n 1	19.26	7.08	19.59	90.00	73.85	90.00	-143.11
M540	C 1 2/c 1	11.56	7.57	30.07	90.00	80.49	90.00	-142.79
M1918	P -1	11.45	5.56	11.66	99.93	61.94	89.82	-142.76
M5643	P 1 21 1	5.01	31.12	8.79	90.00	67.22	90.00	-142.66
M333	P -1	8.81	10.21	7.71	86.73	71.56	101.68	-142.45
M3317	P 1 21/c 1	7.87	7.25	23.19	90.00	73.51	90.00	-141.72
M223	P -1	7.52	7.43	12.62	87.76	64.68	85.16	-140.94
M497	P -1	8.14	8.52	9.91	70.08	96.15	82.73	-140.70

M282	P -1	10.29	7.98	8.51	86.91	75.86	68.27	-140.55
M1982	P -1	7.44	11.86	8.25	105.96	99.02	67.13	-140.49
M14	P -1	7.42	9.67	9.49	76.26	78.37	100.69	-140.46
M1557	P 1 21/c 1	11.38	5.56	20.11	90.00	94.19	90.00	-140.41
M638	P 1 21 1	11.63	14.92	7.55	90.00	102.42	90.00	-140.39
M979	P b c a	20.78	14.76	8.14	90.00	90.00	90.00	-140.31
M5581	C 1 2/c 1	10.76	12.12	20.36	90.00	100.79	90.00	-140.22
M1249	P 1 21/c 1	14.99	7.74	10.99	90.00	95.14	90.00	-140.15
M747	C 1 2/c 1	13.73	7.12	26.85	90.00	82.50	90.00	-139.72
M5471	P 1 21/c 1	4.98	13.03	19.84	90.00	84.56	90.00	-139.49
M3912	P -1	14.34	28.25	4.26	152.72	54.92	125.51	-139.35
M6122	P n a 21	7.16	15.40	23.37	90.00	90.00	90.00	-139.31
M3365	P -1	19.64	4.28	13.44	73.46	48.37	104.81	-139.28
M364	P 1 21/c 1	7.73	7.16	23.50	90.00	95.79	90.00	-139.27
M7509	P n a 21	15.41	7.16	23.37	90.00	90.00	90.00	-139.26
M1682	C 1 2/c 1	13.14	7.03	29.19	90.00	101.17	90.00	-139.22
M1556	C 1 2/c 1	22.23	5.21	23.59	90.00	112.91	90.00	-139.15
M3896	P -1	4.19	19.37	11.79	43.92	91.14	79.51	-139.00
M7947	I 1 2/c 1	21.90	5.86	23.44	90.00	117.12	90.00	-138.88
M58	P 1 21/c 1	4.93	22.32	13.20	90.00	115.84	90.00	-138.80
M4361	P 1 c 1	5.54	11.45	21.50	90.00	108.28	90.00	-138.76
M550	P 1 21/c 1	11.94	14.14	8.10	90.00	72.00	90.00	-138.74
M109	C 1 2/c 1	28.65	3.98	23.02	90.00	106.75	90.00	-138.73
M2968	P 1 c 1	14.48	7.72	14.94	90.00	129.13	90.00	-138.68
M480	P 1 21/c 1	4.02	14.16	21.87	90.00	88.67	90.00	-138.63
M1117	P 1 21/c 1	7.96	22.55	8.17	90.00	60.49	90.00	-138.63
M2103	P 1 21/c 1	10.79	7.51	15.95	90.00	77.92	90.00	-138.62
M251	P 1 21/c 1	11.54	15.09	7.54	90.00	75.52	90.00	-138.44

M490	P 1 21/c 1	7.17	19.14	10.00	90.00	70.98	90.00	-138.29
M3084	P 1 21 1	10.00	19.14	7.17	90.00	109.03	90.00	-138.26
M920	P 1 21/c 1	7.17	19.14	10.00	90.00	70.98	90.00	-138.25
M44	P 1 21/a 1	23.28	4.01	13.83	90.00	80.22	90.00	-138.24
M440	P 1 21/c 1	7.02	7.89	23.33	90.00	80.71	90.00	-138.01
M50	P 1 2/c 1	16.19	4.05	23.08	90.00	123.47	90.00	-137.90
M595	P 1 21/c 1	7.47	15.35	12.19	90.00	65.80	90.00	-137.70
M845	C 1 2/c 1	19.45	7.34	18.82	90.00	105.29	90.00	-137.68
M1634	P 1 21/c 1	11.16	10.27	11.82	90.00	110.47	90.00	-137.68
M144	I 1 2/c 1	26.93	4.07	23.09	90.00	85.11	90.00	-137.67
M68	C 1 2/c 1	31.10	3.97	22.75	90.00	63.75	90.00	-137.65
M677	P 1 21 1	4.06	26.57	11.76	90.00	89.57	90.00	-137.55
M3812	P n a 21	4.00	27.65	22.99	90.00	90.00	90.00	-137.52
M201	P -1	7.15	12.75	8.04	72.56	83.82	109.84	-137.52
M13	P 1 2/c 1	13.51	4.05	23.25	90.00	80.87	90.00	-137.49
M112	C 1 2/n 1	28.92	4.00	22.76	90.00	75.50	90.00	-137.45
M3708	P 1 21 1	23.84	4.05	26.63	90.00	90.00	99.38	-137.44
M1964	P 1 21/c 1	10.69	15.62	7.77	90.00	79.46	90.00	-137.43
M545	P 1 21/c 1	9.22	12.70	11.72	90.00	103.78	90.00	-137.42
M555	P -1	7.77	7.92	11.58	107.02	78.37	75.83	-137.41
M8827	P 1 21 1	24.09	11.72	12.70	90.00	90.00	48.04	-137.40
M1458	P 1 21 1	23.37	27.04	4.04	90.00	80.06	90.00	-137.40
M1024	P 1 21/c 1	7.39	7.68	23.31	90.00	106.74	90.00	-137.34
M4675	P 1 21/c 1	11.07	12.62	10.16	90.00	68.90	90.00	-137.33
M587	P -1	7.92	11.97	7.76	69.13	75.81	67.80	-137.32
M298	P -1	11.89	7.84	12.95	116.15	36.04	108.64	-137.31
M150	P -1	12.39	14.36	4.06	70.67	108.49	106.84	-137.31
M719	P 1 21 1	4.10	26.37	11.73	90.00	90.67	90.00	-137.30

M56	C 1 2/c 1	31.77	3.99	23.09	90.00	118.74	90.00	-137.29
M2683	P 1 21/c 1	12.51	9.46	12.75	90.00	57.82	90.00	-137.29
M1767	P b c a	14.39	22.62	7.79	90.00	90.00	90.00	-137.27
M2734	P b c a	21.26	14.63	8.32	90.00	90.00	90.00	-137.23
M541	P c a 21	3.98	23.16	27.65	90.00	90.00	90.00	-137.22
M4691	P n a 21	27.73	3.99	22.97	90.00	90.00	90.00	-137.22
M659	P b c a	7.79	14.39	22.63	90.00	90.00	90.00	-137.21
M2678	C 1 2/c 1	14.70	19.30	9.13	90.00	82.30	90.00	-137.17
M520	P 1 21/c 1	11.21	12.73	9.98	90.00	68.89	90.00	-137.16
M12	P 1 21/c 1	4.16	13.87	21.50	90.00	90.77	90.00	-137.08
M6554	P 1 21/c 1	4.81	12.72	22.85	90.00	68.21	90.00	-137.06
M611	P 1 c 1	4.05	11.77	27.32	90.00	77.82	90.00	-137.02
M1811	C 1 2/c 1	18.55	7.18	20.08	90.00	73.23	90.00	-137.02
M3564	P -1	7.82	11.74	7.79	71.94	103.81	79.24	-137.00
M2121	P 1 21/a 1	18.29	4.83	15.12	90.00	76.27	90.00	-136.99
M593	P -1	11.66	15.60	3.99	99.74	89.33	117.80	-136.99
M388	P 1 21/c 1	17.14	4.01	22.56	90.00	125.03	90.00	-136.89
M361	C 1 2/c 1	18.50	7.16	20.30	90.00	72.72	90.00	-136.87
M268	P 1 2/n 1	22.89	4.05	14.23	90.00	72.49	90.00	-136.82
M542	P n a 21	23.07	27.12	4.03	90.00	90.00	90.00	-136.80
M414	P 1 2/c 1	11.76	4.04	30.38	90.00	118.30	90.00	-136.76
M148	C 1 2/c 1	27.20	4.04	23.13	90.00	85.40	90.00	-136.74

Table S26. CEL for TFA at the PCM level of theory.

Label	Space Group	a /Å	b /Å	c /Å	α /°	β /°	γ /°	Lattice Energy /kJ/mol
T9	P 1 21/c 1	7.11	7.56	23.01	90.00	82.00	90.00	-149.34
T4121	P 1 21 1	8.69	31.65	4.86	90.00	69.09	90.00	-148.70
T495	P -1	4.83	8.47	15.78	79.68	88.87	100.63	-148.21
T2	P -1	4.82	24.48	20.70	107.16	127.54	122.26	-148.18
T1661	P -1	7.34	13.69	7.44	97.07	94.32	122.49	-147.68
T1487	P -1	7.55	11.15	10.15	47.82	75.19	77.79	-147.45
T93	C 1 2/c 1	7.80	11.61	27.62	90.00	86.75	90.00	-147.34
T917	P -1	7.10	7.05	13.98	102.82	80.97	112.89	-146.95
T283	P 1 21/c 1	3.87	22.07	15.49	90.00	110.63	90.00	-146.94
T3074	P -1	7.74	7.89	11.45	79.88	98.35	65.03	-146.72
T435	P -1	7.52	7.83	11.75	72.58	103.88	78.74	-146.42
T1283	P 1 21/c 1	14.40	7.62	14.86	90.00	129.57	90.00	-145.81
T61	P 1 21/c 1	3.91	14.32	22.06	90.00	93.08	90.00	-145.36
T4972	P 1 21/c 1	7.11	23.56	7.45	90.00	89.40	90.00	-145.20
T10764	P 1 21/n 1	7.85	7.24	21.98	90.00	92.48	90.00	-145.08
T5712	C 1 2/c 1	24.74	6.81	16.29	90.00	66.65	90.00	-145.08
T192	P -1	10.65	6.29	11.22	70.37	107.00	75.36	-145.01
T1332	P 1 21/c 1	11.30	15.32	7.35	90.00	77.81	90.00	-144.94
T5102	P 1 21/c 1	10.47	8.04	14.91	90.00	101.66	90.00	-144.79
T6551	P 1 21/c 1	11.83	6.80	16.31	90.00	106.71	90.00	-144.51
T2259	P 1 21/c 1	15.88	7.75	10.16	90.00	94.08	90.00	-144.22
T4809	P 1 21 1	6.33	29.96	7.10	90.00	70.40	90.00	-144.13
T20	P -1	14.15	37.43	7.71	64.29	122.00	58.72	-144.10
T559	P -1	7.27	12.01	7.71	90.90	88.26	66.11	-144.00

T1465	P 1 21/c 1	10.93	10.79	11.40	90.00	65.52	90.00	-143.79
T273	P 1 21/c 1	13.45	7.00	15.75	90.00	58.73	90.00	-143.63
T2620	P b c a	7.45	14.60	22.81	90.00	90.00	90.00	-143.63
T158	P 1 21/c 1	11.05	10.32	12.08	90.00	113.56	90.00	-143.50
T646	P -1	9.00	10.74	6.78	76.63	85.15	87.05	-143.49
T1729	P 1 21 1	9.89	33.39	3.92	90.00	103.29	90.00	-142.96
T1088	P -1	16.82	9.79	3.92	98.57	98.01	77.83	-142.88
T1021	P 1 21/c 1	10.91	15.06	7.66	90.00	80.63	90.00	-142.82
T983	C 1 2/c 1	11.55	7.70	29.67	90.00	78.99	90.00	-142.74
T402	P 1 21/c 1	11.35	5.81	18.92	90.00	95.51	90.00	-142.67
T240	P 1 21/c 1	9.67	4.83	28.08	90.00	78.23	90.00	-142.62
T557	P -1	7.13	10.11	11.90	70.95	97.81	128.50	-142.34
T3041	P c a 21	15.41	7.10	23.14	90.00	90.00	90.00	-142.28
T22	C 1 2/c 1	28.88	3.84	23.10	90.00	71.80	90.00	-142.05
T1515	C 1 2/c 1	23.91	7.43	15.02	90.00	68.53	90.00	-141.98
T62	P 1 21/c 1	3.95	23.69	13.50	90.00	84.82	90.00	-141.94
T7232	P -1	9.52	10.77	7.66	122.58	93.17	72.87	-141.78
T253	C 1 2/c 1	22.53	7.74	14.43	90.00	83.62	90.00	-141.63
T250	P 1 2/c 1	13.45	4.02	23.10	90.00	80.60	90.00	-141.56
T2912	P 1 21/c 1	8.61	13.67	12.05	90.00	62.37	90.00	-141.43
T669	P -1	11.97	8.37	9.73	130.47	57.23	110.03	-141.36
T465	P 1 21/c 1	12.21	4.88	23.07	90.00	71.54	90.00	-141.31
T845	C 1 2/c 1	16.00	7.51	23.94	90.00	120.22	90.00	-141.06
T40	P 1 21/c 1	15.39	4.75	18.19	90.00	76.55	90.00	-141.05
T1494	P 1 21/c 1	4.85	9.57	27.70	90.00	83.32	90.00	-141.04
T1594	P 1 21 1	11.82	14.84	7.72	90.00	69.44	90.00	-140.96
T130	P -1	4.12	13.03	11.82	97.48	91.99	89.35	-140.94
T34	P 1 21/c 1	13.97	3.86	23.32	90.00	101.56	90.00	-140.94

T279	P 1 2/n 1	16.44	4.01	19.09	90.00	80.59	90.00	-140.92
T356	l 1 a 1	29.29	3.82	22.96	90.00	71.75	90.00	-140.84
T31	P -1	11.60	3.85	14.43	83.24	73.42	91.25	-140.82
T233	P 1 21/c 1	7.25	7.69	23.64	90.00	68.53	90.00	-140.79
T10047	P 1 21/c 1	11.45	7.74	24.89	90.00	34.97	90.00	-140.78
T82	C 1 2/c 1	26.97	4.80	20.63	90.00	74.48	90.00	-140.64
T1217	P 1 21/c 1	4.92	22.39	12.43	90.00	69.88	90.00	-140.56
T2264	C 1 c 1	7.73	22.77	14.26	90.00	84.09	90.00	-140.55
T1778	P 1 21/c 1	11.51	15.02	7.50	90.00	77.40	90.00	-140.48
T1371	P 1 c 1	5.75	11.38	19.97	90.00	76.12	90.00	-140.48
T650	P 1 21/c 1	7.62	7.16	23.29	90.00	99.84	90.00	-140.41
T574	C 1 c 1	3.91	19.12	38.81	90.00	62.18	90.00	-140.38
T41	C 1 2/c 1	16.63	4.68	33.84	90.00	101.05	90.00	-140.26
T219	P b c n	15.28	12.41	13.49	90.00	90.00	90.00	-140.16
T4491	P 1 21 1	7.74	14.87	11.65	90.00	71.96	90.00	-140.11
T762	C 1 2/c 1	16.29	12.37	13.59	90.00	108.26	90.00	-140.03
T202	l 1 2/c 1	26.91	3.98	23.20	90.00	85.95	90.00	-140.00
T509	P 1 21/c 1	5.00	12.78	19.85	90.00	85.75	90.00	-139.98
T211	C 1 2/c 1	15.77	4.82	34.85	90.00	98.38	90.00	-139.91
T1408	P -1	7.43	11.17	8.36	79.10	99.68	74.27	-139.88
T578	P c a 21	3.85	23.22	27.80	90.00	90.00	90.00	-139.88
T96	P -1	3.96	11.79	13.63	78.38	87.65	90.60	-139.86
T995	P n a 21	26.99	3.97	22.99	90.00	90.00	90.00	-139.86
T2022	P 1 21 1	11.77	26.79	3.95	90.00	88.38	90.00	-139.84
T1320	C 1 2/c 1	19.08	3.92	35.79	90.00	104.67	90.00	-139.83
T688	P b c a	33.63	7.89	9.64	90.00	90.00	90.00	-139.82
T70	P 1 21/c 1	3.92	13.87	23.45	90.00	88.79	90.00	-139.77
T51	C 1 2/c 1	28.93	3.84	22.79	90.00	77.33	90.00	-139.70
T52	C 1 2/c 1	32.36	3.85	23.27	90.00	59.51	90.00	-139.69

T2852	C 1 2/c 1	27.09	3.98	34.25	90.00	137.81	90.00	-139.65
T3294	P b c a	31.58	7.68	10.49	90.00	90.00	90.00	-139.61
T638	C 1 2/c 1	19.15	3.93	34.52	90.00	80.33	90.00	-139.59
T1731	C 1 2/c 1	14.14	7.39	26.36	90.00	74.86	90.00	-139.59
T1040	P 1 2/c 1	11.79	3.91	30.59	90.00	118.03	90.00	-139.57
T713	P 1 21/c 1	14.02	3.86	22.98	90.00	85.85	90.00	-139.57
T1846	P b c a	27.90	19.75	4.87	90.00	90.00	90.00	-139.55
T555	P 1 21/c 1	4.99	11.69	22.15	90.00	76.40	90.00	-139.52
T567	P c a 21	7.50	24.03	14.12	90.00	90.00	90.00	-139.51
T684	P 1 21 1	3.97	26.65	11.79	90.00	90.73	90.00	-139.50
T145	C 1 2/c 1	23.49	5.91	21.33	90.00	118.56	90.00	-139.49
T58	P 1 21/n 1	17.37	3.85	18.89	90.00	78.14	90.00	-139.47
T5238	P 1 21/c 1	4.76	15.34	24.11	90.00	132.23	90.00	-139.46
T170	P b c a	14.67	7.91	21.61	90.00	90.00	90.00	-139.46
T111	P 1 21/c 1	12.07	7.57	16.82	90.00	124.43	90.00	-139.34
T1253	P 1 21/c 1	4.74	18.34	15.34	90.00	78.56	90.00	-139.34
T833	P 1 21/c 1	8.62	13.08	14.95	90.00	48.89	90.00	-139.26
T596	C 1 2/c 1	27.14	3.96	23.11	90.00	86.56	90.00	-139.26
T5759	P -1	14.31	4.02	17.17	82.94	63.21	124.10	-139.25

Table S27. CEL for FFA at the PCM level of theory.

Label	Space Group	a /Å	b /Å	c /Å	α /°	β /°	γ /°	Lattice Energy /kJ/mol
F748	P 1 21/c 1	10.77	10.40	11.75	90.00	111.13	90.00	-152.06
F826	P -1	7.71	7.89	12.31	120.61	104.78	85.72	-150.65
F88	P -1	7.98	10.19	9.56	60.32	103.12	80.34	-150.18
F560	P 1 21/c 1	12.24	7.91	12.82	90.00	85.07	90.00	-149.36
F534	P -1	11.84	11.64	7.05	64.22	89.03	128.77	-149.12
F1108	P -1	6.92	11.52	11.33	55.37	92.84	117.74	-148.61
F1115	P b c a	13.72	22.49	8.09	90.00	90.00	90.00	-148.14
F612	P 1 21/c 1	4.57	14.61	19.22	90.00	79.21	90.00	-148.02
F833	P 1 21/c 1	8.64	8.64	17.22	90.00	76.98	90.00	-147.31
F1371	P 1 21/c 1	9.34	9.42	14.02	90.00	88.64	90.00	-147.13
F532	P b c a	14.22	8.25	21.71	90.00	90.00	90.00	-145.92
F1499	P b c a	8.27	35.15	8.71	90.00	90.00	90.00	-145.90
F1439	P 1 c 1	11.02	7.66	15.70	90.00	69.81	90.00	-145.85
F817	P 1 21/c 1	4.41	14.56	20.41	90.00	73.60	90.00	-145.54
F580	P 1 21/c 1	4.57	19.98	13.98	90.00	92.37	90.00	-145.28
F236	P 1 21/c 1	4.55	18.61	15.28	90.00	76.48	90.00	-145.22
F533	P -1	10.12	16.91	4.67	60.67	111.75	115.67	-144.80
F1142	C 1 2/c 1	7.88	22.67	14.44	90.00	77.90	90.00	-144.43
F385	P 1 21/c 1	11.13	13.76	8.43	90.00	78.61	90.00	-144.28
F456	P 1 21/c 1	15.28	4.76	21.76	90.00	54.35	90.00	-144.27
F110	P -1	7.86	12.98	7.62	66.33	77.95	107.98	-144.24
F1510	P 1 21/c 1	4.75	17.08	15.13	90.00	76.74	90.00	-144.09
F1657	P -1	13.69	16.53	11.54	98.80	92.11	105.02	-144.01
F214	P -1	9.60	9.04	8.84	79.07	74.73	58.65	-143.89
F283	P b c a	15.79	9.69	16.56	90.00	90.00	90.00	-143.87

F1956	P -1	4.68	15.74	8.77	96.27	100.69	77.74	-143.84
F287	P -1	4.75	14.25	11.45	63.99	64.84	75.44	-143.71
F1842	P 1 21/c 1	4.71	20.31	13.41	90.00	80.98	90.00	-143.67
F49	P 1 21/c 1	9.64	14.00	9.25	90.00	83.08	90.00	-143.51
F486	P 1 21/c 1	10.24	24.14	7.45	90.00	43.32	90.00	-143.50
F874	P 1 21/c 1	4.90	14.69	17.45	90.00	89.51	90.00	-143.38
F714	P -1	10.64	7.11	9.08	89.05	110.86	81.97	-143.17
F1248	C 1 2/c 1	7.88	11.55	28.67	90.00	85.75	90.00	-143.16
F918	P 1 c 1	15.17	4.65	19.27	90.00	68.21	90.00	-143.15
F882	P -1	4.78	16.33	9.08	70.93	85.69	107.06	-143.12
F84	P -1	12.29	7.19	7.72	93.48	69.86	78.53	-142.95
F691	P 1 21/c 1	4.87	15.10	17.28	90.00	102.85	90.00	-142.81
F1558	P 1 21/c 1	15.92	4.72	18.35	90.00	112.94	90.00	-142.74
F915	C 1 2/c 1	27.88	4.72	19.79	90.00	74.36	90.00	-142.74
F888	P 1 21/c 1	11.38	15.32	7.53	90.00	77.68	90.00	-142.72
F664	P 1 21/c 1	4.47	22.12	15.31	90.00	124.09	90.00	-142.68
F1579	P b c a	14.44	20.74	8.43	90.00	90.00	90.00	-142.66
F221	P 1 21/c 1	14.17	4.71	20.15	90.00	108.82	90.00	-142.65
F1916	P 1 21/c 1	10.39	4.75	28.30	90.00	113.92	90.00	-142.59
F538	P 1 21/c 1	9.80	15.34	8.67	90.00	107.23	90.00	-142.53
F1541	P 1 21/c 1	10.16	11.38	11.30	90.00	83.43	90.00	-142.52
F1228	C 1 2/c 1	33.73	8.75	8.62	90.00	85.58	90.00	-142.50
F687	P 1 21/c 1	12.08	9.96	11.00	90.00	76.26	90.00	-142.49
F753	P -1	7.28	14.96	9.40	122.91	54.40	127.82	-142.37
F1473	P 1 21/c 1	11.39	12.33	9.35	90.00	72.46	90.00	-142.24
F124	P 1 21/c 1	5.18	23.59	16.15	90.00	40.35	90.00	-142.23
F1484	C 1 2/c 1	24.98	6.83	16.68	90.00	65.50	90.00	-142.21

F1963	P 1 21/c 1	9.67	4.62	29.69	90.00	106.26	90.00	-142.18
F1564	P 1 a 1	19.23	4.60	15.06	90.00	71.58	90.00	-142.15
F1237	P 1 21/c 1	9.07	16.75	8.90	90.00	69.92	90.00	-142.07
F1173	P 1 21/c 1	6.52	28.98	7.88	90.00	60.39	90.00	-142.03
F1402	C 1 2/c 1	19.62	7.58	18.71	90.00	114.12	90.00	-141.88
F1155	P 1 21 1	11.46	15.09	7.41	90.00	99.76	90.00	-141.85
F799	P 1 21/c 1	11.05	8.13	18.10	90.00	127.98	90.00	-141.80
F572	C 1 2/c 1	8.25	22.87	14.08	90.00	73.36	90.00	-141.61
F1696	C 1 2/c 1	17.00	4.71	31.24	90.00	93.09	90.00	-141.58
F97	P 21 21 21	19.38	14.19	4.52	90.00	90.00	90.00	-141.58
F1436	P 1 21/c 1	4.63	12.83	21.53	90.00	95.30	90.00	-141.54
F1414	P 1 21/c 1	14.88	6.59	16.52	90.00	53.14	90.00	-141.52
F896	P 1 21/c 1	9.57	11.77	11.78	90.00	105.44	90.00	-141.43
F31	P -1	10.45	8.79	9.47	63.26	71.62	107.93	-141.43
F232	C 1 2/c 1	20.78	5.09	24.31	90.00	87.19	90.00	-141.36
F1129	P -1	14.97	7.31	6.58	68.28	102.12	88.05	-141.23
F597	P 1 21/c 1	7.04	7.70	24.07	90.00	78.98	90.00	-141.23
F1767	P 1 21/a 1	11.98	5.16	21.34	90.00	108.24	90.00	-141.15
F991	P -1	7.82	7.80	11.17	108.97	75.00	92.81	-141.11
F1387	C 1 2/c 1	20.30	8.21	15.40	90.00	94.72	90.00	-141.06
F620	P 1 21/c 1	9.49	15.76	9.19	90.00	111.87	90.00	-141.05
F1953	P 1 21/c 1	11.75	6.90	16.63	90.00	72.99	90.00	-141.03
F1258	P 1 21/c 1	7.45	22.79	7.62	90.00	97.81	90.00	-141.03
F1888	P c a 21	18.72	4.66	29.11	90.00	90.00	90.00	-140.90
F172	P 1 21/c 1	10.94	14.63	7.69	90.00	81.79	90.00	-140.86
F946	P 1 21/c 1	12.27	15.05	7.14	90.00	79.71	90.00	-140.80
F98	C 1 2/c 1	16.08	7.23	21.95	90.00	81.20	90.00	-140.78

F151	P 21 21 21	4.76	15.28	16.94	90.00	90.00	90.00	-140.76
F1434	C 1 2/c 1	11.39	7.74	29.93	90.00	81.22	90.00	-140.62
F1994	P 1 21 1	4.60	24.31	13.22	90.00	63.25	90.00	-140.61
F806	C 1 2/c 1	25.64	6.72	16.98	90.00	61.66	90.00	-140.59
F209	P 1 21/c 1	7.09	14.78	12.30	90.00	77.59	90.00	-140.44
F339	P b c a	7.26	24.10	14.76	90.00	90.00	90.00	-140.43
F848	P 1 21/c 1	7.12	7.32	24.42	90.00	83.29	90.00	-140.38
F1331	P 1 21 1	4.67	27.74	11.42	90.00	63.76	90.00	-140.33
F1559	P 1 21/c 1	12.11	8.42	14.89	90.00	122.96	90.00	-140.19
F52	P 1 21/c 1	4.68	9.23	29.98	90.00	101.88	90.00	-140.15
F1971	P -1	13.05	10.57	5.27	89.05	78.81	118.73	-140.13
F1412	P 1 21/c 1	4.69	15.49	18.00	90.00	95.92	90.00	-140.07
F383	C 1 2/c 1	28.02	4.62	20.99	90.00	106.32	90.00	-140.07
F522	P 1 21/c 1	4.76	10.28	27.06	90.00	92.64	90.00	-140.07
F238	P -1	8.18	7.29	12.70	73.80	65.31	75.64	-140.05
F585	C 1 2/c 1	18.88	4.87	29.18	90.00	106.05	90.00	-140.01
F914	P -1	12.56	11.21	5.01	108.57	104.19	84.16	-139.89
F345	P 1 21 1	7.57	15.07	12.61	90.00	61.98	90.00	-139.82
F1239	P -1	7.41	10.34	9.13	81.03	79.34	108.98	-139.68
F1174	P 1 21/c 1	4.69	20.72	15.33	90.00	118.71	90.00	-139.61
F71	P 1 21/c 1	7.74	7.24	23.54	90.00	75.20	90.00	-139.59

(1) McConnell, J. F., FZ Company. N-(2, 3-xylyl) anthranilic acid, C₁₅H₁₅NO₂ mefenamic acid. *Cryst.Struct.Commun* **1976**, 5, 861-864.

(2) Lee, E. H.; Byrn, S. R.; Carvajal, M. T., Additive-induced metastable single crystal of mefenamic acid. *Pharmaceutical Research* **2006**, 23, 2375-2380.

(3) SeethaLekshmi, S.; Guru Row, T. N., Conformational Polymorphism in a Non-steroidal Anti-inflammatory Drug, Mefenamic Acid. *Crystal Growth & Design* **2012**, 12, 4283-4289.

(4) Andersen, K. V.; Larsen, S.; Alhede, B.; Gelting, N.; Buchardt, O., Characterization of 2 Polymorphic Forms of Tolfenamic Acid, N-(2-Methyl-3-Chlorophenyl)Anthranilic Acid - Their Crystal-Structures and Relative Stabilities. *Journal of the Chemical Society-Perkin Transactions 2* **1989**, 1443-1447.

- (5) Lopez-Mejias, V.; Kampf, J. W.; Matzger, A. J., Polymer-Induced Heteronucleation of Tolfenamic Acid: Structural Investigation of a Pentamorph. *Journal of the American Chemical Society* **2009**, 131, 4554-4555.
- (6) Krishna Murthy, H. M.; Bhat, T. N.; Vijayan, M., Structure of a new crystal form of 2-[[3-(trifluoromethyl)phenyl]amino]benzoic acid (flufenamic acid). *Acta Crystallographica Section B* **1982**, 38, 315-317.
- (7) Lopez-Mejias, V.; Kampf, J. W.; Matzger, A. J., Nonamorphism in Flufenamic Acid and a New Record for a Polymorphic Compound with Solved Structures. *Journal of the American Chemical Society* **2012**, 134, 9872-9875.
- (8) McConnell, J. F., *Crystal Structure Communications* **1973**, 2, 459.
- (9) Frisch, M. J.; Trucks, G. W.; Schlegel, H. B.; Scuseria, G. E.; Robb, M. A.; Cheeseman, J. R.; Scalmani, G.; Barone, V.; Mennucci, B.; Petersson, G. A.; Nakatsuji, H.; Caricato, M.; Li, X.; Hratchian, H. P.; Izmaylov, A. F.; Bloino, J.; Zheng, G.; Sonnenberg, J. L.; Hada, M.; Ehara, M.; Toyota, K.; Fukuda, R.; Hasegawa, J.; Ishida, M.; Nakajima, T.; Honda, Y.; Kitao, O.; Nakai, H.; Vreven, T.; Montgomery Jr., J. A.; Peralta, J. E.; Ogliaro, F.; Bearpark, M. J.; Heyd, J.; Brothers, E. N.; Kudin, K. N.; Staroverov, V. N.; Kobayashi, R.; Normand, J.; Raghavachari, K.; Rendell, A. P.; Burant, J. C.; Iyengar, S. S.; Tomasi, J.; Cossi, M.; Rega, N.; Millam, N. J.; Klene, M.; Knox, J. E.; Cross, J. B.; Bakken, V.; Adamo, C.; Jaramillo, J.; Gomperts, R.; Stratmann, R. E.; Yazyev, O.; Austin, A. J.; Cammi, R.; Pomelli, C.; Ochterski, J. W.; Martin, R. L.; Morokuma, K.; Zakrzewski, V. G.; Voth, G. A.; Salvador, P.; Dannenberg, J. J.; Dapprich, S.; Daniels, A. D.; Farkas, Ö.; Foresman, J. B.; Ortiz, J. V.; Cioslowski, J.; Fox, D. J. *Gaussian 09*, Gaussian, Inc.: Wallingford, CT, USA, 2009.
- (10) Habgood, M.; Sugdan, I. J.; Kazantsev, A. V.; Adjiman, C. S.; Pantelides, C., Efficient Handling of Molecular Flexibility in Ab Initio Generation of Crystal Structures. *Journal of Chemical Theory and Computation* **2015**, 11, 1957-1969.
- (11) Chisholm, J. A.; Motherwell, S., COMPACT: a program for identifying crystal structure similarity using distances. *Journal of Applied Crystallography* **2005**, 38, 228-231.
- (12) Tkatchenko, A.; Scheffler, M., Accurate Molecular Van Der Waals Interactions from Ground-State Electron Density and Free-Atom Reference Data. *Physical Review Letters* **2009**, 102, 073005.
- (13) Clark, S. J.; Segall, M. D.; Pickard, C. J.; Hasnip, P. J.; Probert, M. J.; Refson, K.; Payne, M. C., First principles methods using CASTEP. *Zeitschrift für Kristallographie* **2005**, 220, 567-570.
- (14) Ambrosetti, A.; Reilly, A. M.; DiStasio, R. A.; Tkatchenko, A., Long-range correlation energy calculated from coupled atomic response functions. *J Chem Phys* **2014**, 140, 18A508.
- (15) Nyman, J.; Day, G. M., Static and lattice vibrational energy differences between polymorphs. *Crystengcomm* **2015**, 17, 5154-5165.
- (16) Williams, D. E.; Cox, S. R., Nonbonded Potentials For Azahydrocarbons: the Importance of the Coulombic Interaction. *Acta Crystallographica Section B - Structural Science* **1984**, 40, 404-417.
- (17) Gilpin, R. K.; Zhou, W., Infrared studies of the thermal conversion of mefenamic acid between polymorphic states. *Vibrational spectroscopy* **2005**, 37, 53-59.
- (18) Mattei, A.; Li, T., Polymorph Formation and Nucleation Mechanism of Tolfenamic Acid in Solution: An Investigation of Pre-nucleation Solute Association. *Pharmaceutical Research* **2012**, 29, 460-470.
- (19) Surov, A.; Szterner, P.; Zielenkiewicz, W.; Perlovicha, G., Thermodynamic and structural study of tolfenamic acid polymorphs. *Journal of Pharmaceutical and Biomedical Analysis* **2009**, 831-840.
- (20) Uzoh, O. G.; Cruz-Cabeza, A. J.; Price, S. L., Is the Fenamate Group a Polymorphophore? Contrasting the Crystal Energy Landscapes of Fenamic and Tolfenamic Acids. *Crystal Growth & Design* **2012**, 12, 4230-4239.
- (21) Lee, E.; Byrn, S., Stabilization of Metastable Flufenamic Acid by Inclusion of Mefenamic Acid: Solid Solution or Epilayer? *Journal of Pharmaceutical Sciences* **2010**, 99, 4013-4022.
- (22) Cruz-Cabeza, A. J.; Reutzel-Edens, S. M.; Bernstein, J., Facts and fictions about polymorphism. *Chemical Society Reviews* **2015**, 44, 8619-8635.

- (23) Stone, A. J.; Dullweber, A.; Engkvist, O.; Frascini, E.; Hodges, M. P.; Meredith, A. W.; Nutt, D. R.; Popelier, P. L. A.; Wales, D. J. *ORIENT: a program for studying interactions between molecules*, 4.8.29; University of Cambridge, 2015.
- (24) Coelho, A. A. *Topas*, 3.1; Bruker AXS GmbH, Karlsruhe, Germany: 2003.
- (25) Shephard, J.; Evans, J.; Salzmann, C., Structural Relaxation of Low-Density Amorphous Ice upon Thermal Annealing. *Journal of Physical Chemistry Letters* **2013**, *4*, 3672-3676.
- (26) Shirley, R. *CRYSFIRE Suite*, 2002.
- (27) Favre-Nicolin, V.; Cerny, R., FOX, 'free objects for crystallography': a modular approach to ab initio structure determination from powder diffraction. *Journal of Applied Crystallography* **2002**, *35*, 734-743.
- (28) Cockcroft, J. K. *PROFIL*, 1998.
- (29) Shard, A. G.; Havelund, R.; Spencer, S. J.; Gilmore, I. S.; Alexander, M. R.; Angerer, T. B.; Aoyagi, S.; Barnes, J.-P.; Benayad, A.; Bernasik, A.; Ceccone, G.; Counsell, J. D. P.; Deeks, C.; Fletcher, J. S.; Graham, D. J.; Heuser, C.; Lee, T. G.; Marie, C.; Marzec, M. M.; Mishra, G.; Rading, D.; Renault, O.; Scurr, D. J.; Shon, H. K.; Spampinato, V.; Tian, H.; Wang, F.; Winograd, N.; Wu, K.; Wucher, A.; Zhou, Y.; Zhu, Z., Measuring Compositions in Organic Depth Profiling: Results from a VAMAS Interlaboratory Study. *The Journal of Physical Chemistry B* **2015**, *119*, 10784-10797.